

General Disclaimer

One or more of the Following Statements may affect this Document

- This document has been reproduced from the best copy furnished by the organizational source. It is being released in the interest of making available as much information as possible.
- This document may contain data, which exceeds the sheet parameters. It was furnished in this condition by the organizational source and is the best copy available.
- This document may contain tone-on-tone or color graphs, charts and/or pictures, which have been reproduced in black and white.
- This document is paginated as submitted by the original source.
- Portions of this document are not fully legible due to the historical nature of some of the material. However, it is the best reproduction available from the original submission.

X-700-76-155
PREPRINT

NASA TM X- 71166

PREDICTION AND MEASUREMENT OF RADIATION DAMAGE TO CMOS DEVICES ON BOARD SPACECRAFT

(NASA-TM-X-71166) PREDICTION AND
MEASUREMENT OF RADIATION DAMAGE TO CMOS
DEVICES ON BOARD SPACECRAFT (NASA) 42 p HC
\$4.00 CSCL 09C

N76-28479

Unclas
G3/33 48569

**R. A. CLIFF
V. DANCHENKO
E. G. STASSINOPOULOS
M. SING
G. J. BRUCKER
R. S. OHANIAN**

JULY 1976



GODDARD SPACE FLIGHT CENTER
GREENBELT, MARYLAND

PREDICTION AND MEASUREMENT OF RADIATION DAMAGE
TO CMOS DEVICES ON BOARD SPACECRAFT

R. A. Cliff, V. Danchenko, E. G. Stassinopoulos, and M. Sing,
Goddard Space Flight Center
Greenbelt, Maryland

G. J. Brucker and R. S. Ohanian
RCA Astro Electronics Division
Princeton, N. J.

JULY 1976

GODDARD SPACE FLIGHT CENTER
GREENBELT, MARYLAND

Abstract

The CMOS Radiation Effects Measurement (CREM) experiment is presently being flown on the Atmosphere Explorer - 55. The purpose of the experiment is to evaluate device performance in the actual space radiation environment and to correlate the respective measurements to on-the-ground laboratory irradiation results. The experiment contains an assembly of C-MOS and P-MOS devices shielded in front over 2π steradian by flat slabs of aluminum of 40, 80, 150, and 300 mils (1.02, 2.04, 3.81, and 7.62 mm) thicknesses, and by a practically infinite shield in the back. This paper presents initial results obtained from the CREM experiment. Predictions of radiation damage to C-MOS devices are based on standard environment models and computational techniques. A comparison of the shifts in CMOS threshold potentials, that is, those measured in space to those obtained from the on-the-ground simulation experiment with Co-60, indicates that the measured space damage is greater than predicted by a factor of two for shields thicker than 100 mils (2.54 mm), but agrees well with predictions for the thinner shields. It is not clear at this time how the trapped particle environment models or the computational methods should be modified in order to achieve better agreement between experimental results and predicted damage curves. A subsequent paper will present some considerations along these lines as well as an evaluation of performance of C-MOS devices located in a typical electronic subsystem box within the spacecraft.

Contents

	<u>Page</u>
1. Introduction	1
2. Experimental Approach and Method	2
3. Description of Devices	2
a. RCA COS/MOS, Type CD 4007AK/IR	3
b. AMI p-channel, Type 585A	3
4. AE-55 Spacecraft, Its Orbit and CREM	3
5. Space Radiation Environment for AE-55	6
6. Dose and Shielding Calculations	7
7. On-the-ground Simulation and Calibration	8
8. Flight Data Results	10
9. Analysis and Discussion	10
10. Conclusion	11
11. Acknowledgements	13
12. References	14

List of Figures

1. Atmosphere Explorer 55.
2. CREM device box and its cover.
3. Device locations in CREM box.
4. Transistor biasing during irradiation.
5. Transistor biasing during measurement.
6. Time history of mission integrated, omnidirectional, integral, trapped electron fluxes.
7. Time history of mission integrated, omnidirectional, integral, trapped proton fluxes.
8. Cumulative sum of mission integrated, omnidirectional, integral, trapped electron fluxes.
9. Cumulative sum of mission integrated, omnidirectional, integral, trapped proton fluxes.
10. Spectral distribution of total mission integrated, omnidirectional, integral, trapped particle fluxes to day 139.
11. Contribution of electrons, protons, and Bremsstrahlung to the total dose-depth curve.
12. Dose-depth curve for slab and spherical geometries.
13. Monte Carlo and AEVDP dose-depth curves.
14. Radiation response of RCA n-channel transistor.
15. Radiation response of RCA p-channel transistor.
16. Radiation response of AMI p-channel transistor.
17. CREM flight data of RCA n-channel transistors.
18. CREM flight data of RCA and AMI p-channel transistors.
19. CREM flight data of RCA n-channel transistors under various shields.
20. Comparison of flight and theoretical data.

1. Introduction

There are many advantages of Complementary Metal-Oxide-Semiconductor (C-MOS) integrated circuits (ICs) over bipolar ICs in the design of large scale integrated logic and memory circuitry for spacecraft. Among these are extreme compactness and low power consumption. Such circuits are being orbited to an ever increasing extent. C-MOS ICs, however, are found to be more sensitive to space radiation than their bipolar counterparts. The mechanism responsible for the radiation damage in C-MOS devices is that of ionization and charge accumulation in the gate oxide and at the semiconductor-insulator interface. These effects begin to appear about two orders of magnitude lower than the effects of semiconductor surface damage in bipolars. In addition, since charge accumulation in the gate oxide is cumulative, the radiation damage in C-MOS ICs has become of great concern as space missions become longer and longer.

The successful application of unhardened C-MOS devices in spacecraft which traverse the Earth's radiation belts may hence require shielding. Shielding, however, is very heavy, and therefore it is most desirable to minimize any excessive weight penalty. It has consequently become important for spacecraft designers to be able to predict accurately the anticipated radiation damage to C-MOS devices and to estimate closely the shielding requirements. Such predictions presuppose that the following three elements are known: (1) the energies of the space radiation encountered by the spacecraft, (2) the shielding effectiveness of given materials for particles of various energies, and (3) the response of C-MOS devices to the radiation which is found inside the shield.

In regards to element (1), even though the best radiation environment models available today have been considered, the electron intensities are known only to within a factor of 3 and the proton intensities to within a factor of 2. These large uncertainties in the flux estimates cannot be resolved by experiments like CREM. As to elements (2) and (3), although the radiation damage in C-MOS as a function of dose in rads can be measured in the laboratory by using such radiation sources as Co-60 or monoenergetic electron accelerators, it is not practical to reproduce the complicated in-orbit particle environment for this purpose or for the purpose of experimentally determining the effectiveness of the shielding material. In addition, there is a long-term annealing process (self healing) of radiation damage active in C-MOS devices which may be different in the space environment than on the ground.

To resolve some of these questions, the C-MOS Radiation Effects Measurements (CREM) experiment is presently being flown on the Atmosphere Explorer 55 (formerly designated AE-E) while simultaneously the necessary complementary measurements are being carried out on the ground. In this paper we present some significant and interesting preliminary results. As more data become available, a more detailed analysis and thorough evaluation will be performed and their findings presented in a subsequent report.

2. Experimental Approach and Method

The essence of this experiment is to "calibrate" the space radiation environment against an on-the-ground monoenergetic radiation source, such as Co-60, or vice versa, using the effects of C-MOS devices, and to compare the calibration results with current model predictions of the space radiation environment, as processed and converted to dose depth concepts by the various computer systems in use today. Since the objective of the experiment is based on measurement and comparison, the devices used must be chosen very carefully so that they will have the same response in radiation environments of the same ionization-producing dose. It would have been ideal to be able to first calibrate the devices and then use the same on board the spacecraft, but, as was shown¹ by one of the authors, the radiation response of MOS devices changes with repeated radiation and annealing cycles. The next best approach is to use devices which are manufactured in the same gate oxide growth process run. This is what was done. In addition, the device radiation response must cover a large radiation dose range in case of under or over prediction of the space radiation environment.

It is known that most of the MOS devices exhibit a long term annealing (some even show reverse annealing) of radiation damage as a function of temperature. Therefore, for the space flight results of the CREM to be meaningful, there must be a number of associative on-the-ground measurements and calibrations, such as on-the-ground simulation experiments whereby the long term annealing will be measured and accounted for.

CREM, therefore, consists of five major parts: (1) the flight apparatus that directly measures the effects of the space radiation environment on C-MOS devices under various shieldings (4 defined and 1 estimated), (2) the laboratory simulation experiment with Co-60 as an on-the-ground calibration source, (3) modeling and prediction of the space radiation environment using the latest available models and the actual orbital parameters, (4) using this predicted space radiation environment, the calculation of dose depth curves for theoretical one-dimensional slab and three-dimensional spherical geometries, and (5) comparison of predicted damage to actual damage in the orbiting devices.

3. Description of Devices

Two MOS technologies were chosen for this experiment: The RCA COS/MOS unhardened or "soft" technology and the AMI p-MOS, high threshold variety. The reasons for choosing these two technologies are: (1) RCA's n-channels of the "soft" variety, when biased with 10 volts, already exhibit a measurable shift in the threshold potential (the gate bias measured at 10_{μ}A drain current) after an exposure of about 1×10^3 rad-silicon (See Figure 14); this permits the measurement of radiation damage at lower ionization doses, in case the space radiation environment has been overestimated. At the same time, the p-channels

of the RCA CD-4007 devices on the same chip of silicon are much less radiation-sensitive, when both biased and unbiased, and will cover the high portion of the dose range; (2) The AE-55 spacecraft contains some RCA "soft" COS/MOS devices and it would be advantageous for the AE project to be able to monitor and predict possible radiation damage to the spacecraft circuitry during this mission. (3) The radiation-sensitivity of the p-channel AMI high-threshold devices (not ion-implanted) lies between that of the RCA biased or unbiased n- and p-channels. Aside from this, GSFC uses a considerable quantity of these devices in its missions and it will, therefore, be of great value to have direct measurements on them in the space environment.

a. RCA COS/MOS, Type DC 4007AK/IR - The RCA COS/MOS integrated circuits, Dual Complementary (Type DC 4007 Pair Plus Inverter) were manufactured by RCA in February 1974 and packaged in welded-seal ceramic flat packs with 3 mil (0.08 mm) Kovar lids [9 mil (0.2 mm) equivalent aluminum]. Each device contains 3 p-channel and 3 n-channel transistors which are individually accessible. The lot (No. 405) was guaranteed by the company to have originated from the same wafer, or from several wafers, but having been physically located next to each other in the same gate oxide growth run. This is important because for the experiment to be meaningful, the radiation-induced gate charge trapping capability of the gate oxides must be the same.

b. AMI p-channel, Type 585A - A wafer containing AMI p-channel, 10 channel switches, was manufactured by AMI in 1971 and diced and packaged at GSFC in 22-lead flat packs with 10 mil (0.3 mm) Kovar lids [28 mil (0.7 mm) equivalent Al]. All the devices came from the same wafer. In this configuration, each device contains 10 individually accessible p-channel transistors (although only 6 of them were actively used). The threshold potentials were around -4 volts and the variation in the threshold potential from transistor to transistor in the same device was within 0.2 volts. In this particular technology the radiation response in the unbiased devices is greater than in the biased devices.

The uniformity of the charge trapping capability has been determined by irradiating 6 devices of each type with Co-60 gamma rays and with 1 MeV electrons. The variation in the shift of the threshold potentials (ΔV_{GT}) was found to be less than 5% from device to device in both technologies.

4. AE-55 Spacecraft, Its Orbit and CREM

The main purpose of the Atmosphere Explorer 55, Fig. 1, is to explore the thermosphere on a global basis. Its shape is a 16-sided polyhedron and it weighs about 1,625 pounds (737 kilograms). The spacecraft was launched on November 19, 1975, and achieved its original, highly elliptical, orbit with an apogee of 1,864 statute miles (3,000 kilometers) and a perigee of 98 miles (157 kilometers). The orbit is inclined 19.7° to the equator.

Because of its main objective of thermosphere exploration, the spacecraft's apogee was allowed to decrease by about 2 to 5 km per day until it was stabilized on May 15, 1976 with an apogee of 1,600 km and perigee of 151 km. On August 1, 1976, the orbit will be circularized at 300 km.

The on-board CREM experiment consists of: (a) the device assembly, mounted flush with the solar array in the surface of the spacecraft, as shown in Fig. 1, and containing four device groups; (b) an additional fifth device group located within a typical electronics box inside the spacecraft; and (c) an on-board data acquisition system, also located inside the spacecraft.

Each device group contains 26 instrumented transistors: 6 AMI p-channels (one AMI 585A device), 10 RCA p-channels and 10 RCA n-channels (4 RCA 4007 devices). A total of $5 \times 26 = 130$ instrumented transistors are in the CREM experiment on the spacecraft. The locations of the devices in the CREM device box are shown in Figs. 2 and 3.

Shielding of devices. The devices in the box are mounted on a printed circuit board with copper heat sink slabs bonded to the back of the board. This printed circuit board is assembled into the device box as follows: The board forms the front of a rectangular prism, the other 5 sides of which are made of 250 mil (6.4 mm) aluminum bonded to 250 mil (6.4 mm) thick tungsten. This gives a 2π steradian back shield of equivalent thickness greater than 1.8 inch (4.6 cm) of aluminum. A front cover is mounted over the printed circuit board. This cover provides aluminum shields of thicknesses 40 mil (1.0 mm), 80 mil (2.0 mm), 150 mil (3.8 mm), and 300 mil (7.6 mm) designed in such a way that behind each shield thickness there is one group of four RCA 4007 devices and 1 AMI p-channel device. [When calculating shield thicknesses, however, the device package lids of 9 mil (0.2 mm) equivalent aluminum was added to each nominal slab thickness in the CREM box for the RCA devices. The AMI device package requires a value of 28 mil (0.7 mm) of Al.] The entire device box was then mounted with the printed circuit board in the plane of the surface of the spacecraft. The device box in combination with the body of the spacecraft forms a 2π steradian back shield, which is for practical purposes infinitely thick compared to the front shields. The front of the box has an unobstructed 2π steradian view of the space environment.

Device biasing. The electronics box on the spacecraft is designed to continuously apply a selected gate-to-substrate bias to each device except during the brief interval ($\frac{1}{2}$ second) during which that particular device is being measured. Of the 6 AMI transistors in each device group, 3 are at a constant $V_G = 0$ V and 3 are at $V_G = -10$ V. Of the 10 RCA p-channel transistors in each device group, 2 are at a constant $V_G = 0$ V, 2 are at a constant $V_G = -10$ V, 4 are at V_G which is zero volts for half

the orbit and -10 V the other half of the orbit, and 2 are connected in a selfbiasing arrangement. (The duty cycled and self-biasing transistors will not be further discussed in this paper.) The 10 RCA n-channel transistors in each device group are biased like the 10 p-channel transistors except that $V_G = +10$ V replaces $V_G = -10$ V. Fig. 4 shows the bias circuits for both p- and n-channel transistors.

Device Measurement. When the command to measure the devices is executed (from the ground or from an on-board programmer), the CREM electronics box automatically sequences through a complete measurement cycle of the 130 transistors. In each transistor, the 8 gate-to-substrate biases (V_G 's) required to produce 8 predetermined values of drain current, I_D , are measured. They range from 1 μ A (nearly cut off) to 3 mA (actively switching) with intermediate current values of 3 μ A, 10 μ A, 30 μ A, 100 μ A, and 1 mA. In this way I-V plots can be obtained for the individual n- and p-channel transistors. The measurements are made by forcing the selected test current through the transistor and using an operational amplifier feedback circuit to adjust V_G to the value which maintains $V_D = 10$ V. Fig. 5 shows such circuits for both n- and p-channel transistors. In this discussion, only the essential elements of the measurement process have been covered; other elements (e.g. stability) which increase the complexity of the actual circuit, will not be considered here. The details of the measurement technique will be covered in a separate paper.

Measurement accuracy. Considerable attention has been given to controlling and minimizing possible errors inherent in the measurements. Each device package is thermally bonded to a heat sink, thus keeping all the devices within 1.4°C. of each other. Four thermistors are used to measure and telemeter the temperature of various parts of the heat sink in order to verify its proper function. Electrical switching, associated with the biasing and measurement function, is accomplished by using reed relays which, for practical purposes, act as ideal switches: zero resistance when closed and zero leakage when open. The measured gate voltage is sent directly to the telemetry system. The single-sample random errors and the quantization errors associated with the telemetry system are less than ± 30 mV. Several sources can contribute to errors in the values of the test currents, as for example, leakages in the back-biased parasitic diodes which exist on the sample IC chips. These would subtract from actual sample device current. However, both the thermally and radiation induced leakage are orders of magnitude smaller than the smallest test current used. The operational amplifier input current subtracts from the test current; however, the CREM instrument is calibrated prior to use and only the changes in this current introduce errors. Likewise, changes in operational amplifier offset voltage, and changes in precision current source reference voltage will introduce errors. An in-flight calibration scheme is employed to measure changes in each of these variables. The actual value of each

test current is within $\pm 16\%$ of the nominal value (the $10 \mu\text{A}$ test current is within $\pm 1\%$ of its nominal value), but the actual value of each current is known and constant within $\pm 1\%$.

5. Space Radiation Environment for AE-55

Starting from the launch date (November 19, 1975) and extending to mission date 159 (April 26, 1976), a continuous trajectory ephemeris was generated by the Telemetry Computation Branch at Goddard, in which the actual satellite positions were defined in polar space at two-minute intervals. This continuous flight path description was divided into 159 trajectory segments of 24 hour duration that were subsequently converted into magnetic B-L space with McIlwain's INVAR program of 1965² and the field routine ALLMAG³ utilizing the IGRF (1965) geomagnetic field model⁴. The field coefficients were extrapolated to the true mission epoch 1975.11 with linear time terms representing secular variation effects. Orbital flux integrations were then performed for each of these segments with the UNIFLUX system⁵ using standard models of the environment: the appropriate for the launch epoch solar-min. versions of the AE5 and AE4⁶ for the inner and outer zone electrons, and the AP7 and AP8 for the medium and high energy protons. All are static models which do not consider temporal variations. It should be noted that the AE5 does not contain any "Starfish" residuals because the artificial component contained in the experimental data used in the construction of the model, was exponentially decayed during the modelling process down to about background levels with lifetimes and cutoff times available as functions of energy and magnetic shell parameters L ⁹.

The daily electron and proton integration results are shown in Figs. 6 and 7, respectively, for several energy levels. The data represent averaged, surface incident, omnidirectional, integral intensities. The periodic pattern in the contours is believed to be produced by the precession of the decaying eccentric orbit through the asymmetric (anomalous) geomagnetic geometry configuration. The trapped particle fluxes, predicted by the standard environment models for the AE-55 trajectory, do not seem to decline significantly for the first 150 days of the mission, although apogee altitude dropped from about 3000 km to about 1835 km. This is true for both species of particles, for all but the lowest energies plotted. After day 150, a more rapid decrease in the total daily intensities is indicated.

Figs. 8 and 9 depict the total vehicle encountered fluxes as a function of time. In these graphs, for every day in the mission, the cumulative sum of particles up to that date is given at the selected energies. The integral proton and electron spectra for the respective cumulative sums on day 139 are given in Fig. 10.

Although the best available data were used in the calculations, the accuracy of the results is not better than a factor of 3 for the electrons and a factor of 2 for the protons.

Solar flare protons are of no concern to this analysis because the mission is flying during the inactive period of the solar cycle.

6. Dose and Shielding Calculations

In a previous paper¹⁰, the techniques for computing dose-depth curves for any assumed radiation environment were described. These techniques are applied to the three radiation environments (after 48, 88, and 139 days in orbit, Table 1) by using three different approximation methods, described in the following sections.

One-dimensional slab geometry. The calculations from one-dimensional radiation transport theory with slab geometry and infinite back shielding, representing the total accumulated theoretical dose from the electron and proton environments as a function of equivalent aluminum thickness (including device package lids), have been performed for the indicated mission dates and for the constant biased RCA n-channel devices located at the F3 positions (see Fig. 3). Fig. 11 shows the total dose-depth curve after 48 days in orbit with all the contributing components, including bremsstrahlung. Clearly, both electron and proton contributions towards the total dose for the 40 mils (1. mm) and 80 mils (2. mm) shields are equally significant, whereas only protons contribute to the total dose for the 150 mils (3.8 mm) and 300 mils (7.6 mm) shields. Fig. 12 shows the total dose depth curves for the three environments.

Three-dimensional spherical geometry. The real spacecraft geometry, however, is not one- but three-dimensional and consequently the curves of Fig. 12 are only crude approximations to the true physical situation. In order to improve on these approximate solutions, a three-dimensional spherical shielding evaluation was performed, which takes into account not only all the shielding provided by the spacecraft itself, the adjacent on-board experiment instruments, the diverse device packages, the p-c board, the brackets, etc., but also the lack of shielding, if such exists. The calculations were carried out with a computer code called Modified Elemental Volume Dose Program (MEVDP)¹¹. This code is based on a three-dimensional ray tracing technique which determines the elemental solid angle subtended at the device for any direction, shield thickness, and material. The program makes it possible to model any geometrical shape, either solid or void, which makes up the shield complement. Application of MEVDP to the CREM experiment yielded the theoretical doses shown in Fig. 12 for the three selected radiation environments, in comparison to the doses obtained from the one-dimensional slab geometry. Table 2 contains the theoretical spherical doses for all twenty devices in the CREM box, as of mission day 139. Predicted doses are consistently similar within each group except at location F5 in Group 1 and in Group 2, which are significantly different. It is believed that this difference is due to the thicker package lid of the AMI devices (F5). The voltage shifts

of the p-channels are so small that the dose measurements are not yet meaningful. These transistors will contribute usable results later in the mission as the total dose increases.

Monte Carlo method. The error introduced into the results by the calculational techniques applied in this analysis can be estimated through a comparison with data obtained from another method which is known to be more accurate: the Monte Carlo electron transport evaluation. The Theoretical Radiation Group at AFWL¹² provided such a dose depth curve for the 139-day electron spectrum which was calculated with their modified version of the Tiger Code^{13,14}. Fig. 13 shows that curve in addition to the corresponding data obtained by the simpler technique described in the previous section. It can be seen that the simple-approach solutions consistently underestimate the doses: by about 40% at shield thicknesses of 50 mils and by about 20% for the thick shields. Corrections to the electron dose contributions were subsequently made to all theoretical values derived from the three-dimensional spherical geometry method. In this study only aluminum shielding materials were considered.

7. On-the-ground Simulation and Calibration

In order to calibrate the space radiation environment against the GSFC Co-60 source, or vice versa, and in order to ascertain the extent of long-term annealing, the on-the-ground CREM experiment was started as soon as enough data had been received from space to establish the trend in the radiation damage there. The sample devices for this experiment were chosen, as previously described, to be as identical as possible to the ones on the CREM unit on board the spacecraft and the data were recorded in an identical way with the breadboard of the CREM instrument.

The Co-60 gamma ray flux was measured with a Victoreen Type 555 Radacon II Integrated Rate Meter. Shortly before the experiment was activated, the calibration of these probes was checked by Victoreen with a gamma source calibrated by NBS and certified to be correct within 5%.

The on-the-ground simulation experiment involved the irradiation of one group of samples (i.e., a group of devices similar to the ones under each shield thickness on board the AE-55) every week with a weekly dose of Co-60 radiation in such a way as to effect the same radiation damage on the laboratory devices as the actual damage initially observed in space. Between weekly irradiations, the test devices were permitted to anneal at room temperature and under the same biasing configuration as in space. Data readings were taken regularly just before each next irradiation.

Since the range of temperature variation experienced by the CREM assembly in space is rather narrow (150 - 30°C) and lies in the vicinity of room temperature, it is safe to assume, on the basis of earlier work¹⁵, that the degree of long term annealing, if any, will be similar in the present experiment, and that it can therefore be eliminated as an unknown quantity.

Some results of the calibration and simulation are shown in Fig. 14 for RCA n-channels, biased and unbiased, where the circles relate to data obtained each week from the regularly irradiated devices (simulation). For comparison purposes, average results from a fast-rate radiation response on six n-channels of three independent samples, all irradiated so as to receive the entire corresponding dose within one day, are also given in Fig. 14 by the crosses. In this figure, gate biases for 10 μ A currents are plotted against the total accumulated dose in rad-silicon and against the number of days in orbit, for an assumed constant dose in space. Since there is a slight variation in the initial threshold potentials from device to device, the data were normalized to the same initial threshold potential. As can be seen from the graph, the radiation response for a biased n-channel is linear for both the fast and the simulation rate modes. In the simulation rate curve the lower circles are the threshold potentials immediately after the weekly irradiations and the upper ones are after weekly annealings, so that the true simulation rate response is represented by the line drawn through the upper data circles. The samples of the on-the-ground experiments were subjected to the same radiation dose every week. This is because in this mission the orbit was continually changing and precise orbit parameters were not known a priori.

When it was observed that the total accumulated dose exceeded the one in space, the irradiations were stopped at a total dose of 2.4×10^4 rad-silicon (see Fig. 14) and only annealing was observed thereafter. As can be seen, the pure annealing also shows a linear behavior and constitutes about 0.9 mV per day for RCA biased n-channels. This very slow recovery characteristic of these RCA oxides has also been demonstrated elsewhere.¹⁶ The behavior of the unbiased n-channels, as shown in the same graph, is not linear and the shifts in the threshold potential are considerably smaller.

Figs. 15 and 16 show similar examples for RCA and AMI unbiased and biased p-channels. The general response of these samples is not linear and one observes almost no measurable annealing in RCA p-channel devices. In AMI devices, a considerable annealing is observed in the unbiased state, but almost no annealing in the biased state. There is a greater scattering of the data of these devices than in the RCA p-channels.

With these parallel on-the-ground measurements available, in particular the simulation dose rate curves, it is now possible to directly evaluate the total accumulated radiation dose sustained by the devices in space, behind the various aluminum shield thicknesses, under the assumption, of course, that the space-borne devices have an identical radiation response.

8. Flight Data Results

The data of the flight experiment, as received from the spacecraft, consist of actual gate potential measurements for the 8 specified drain currents of the individual MOS transistors. The data shown in Figs. 17, 18, and 19 depict the shifts of the 10 μ A drain current gate potentials as a function of number of days in orbit. Fig. 17 is for biased and unbiased RCA n-channel transistors. In comparison to the on-the-ground experiments where the radiation response for the biased n-channel is linear, the response in space is not linear. This is because the orbit of the AE-55 spacecraft was continually evolving into a less eccentric one with a corresponding decrease in energetic particle density encountered. Fig. 18 shows a similar degradation in the actual threshold potentials for RCA and AMI p-channels in both biased and unbiased configurations. Fig. 19 represents the results of biased n-channel devices under the various aluminum shield thicknesses of the experiment.

From the flight data of Fig. 19 and the on-the-ground simulation data of Fig. 14, the respective doses for each mission duration have been calculated and are plotted in Fig. 20. It should be recalled that all these data were obtained from the degradation of n-channels biased with 10 volts and that the devices were exposed to worst case gate biasing conditions. Consequently, these larger threshold voltage shifts give a more sensitive measurement of ionization dose. The unbiased n-channel and p-channel results are not yet usable since the threshold voltage shifts to date are too small.

9. Analysis and Discussion

Space flight data already received from the CREM instrument have permitted a much closer estimation of the penetration and ionization capacity of the space radiation environment, leading to some reduction in the uncertainty factors associated with the prediction of radiation damage in C-MOS devices. As more flight data becomes available and the orbital parameters for this spacecraft are further determined and analyzed, it may be possible to reduce the uncertainty factors even further.

It is estimated that the CREM flight data, such as shown in Figs. 17, 18, and 19, are correct to within 10%. This uncertainty is due mainly to the temperature variations of the devices during the data read-out and to a lesser extent due to errors in the CREM data acquisition system and the spacecraft's telemetry systems. The former is yet to be analyzed.

In the case of the on-the-ground simulation and calibration data, although the accuracy of the CREM breadboard is within 1%, Co-60 calibration is within 5%, and the variation from sample to sample was found to be also within 5%. The total error, therefore, is approximately within 10%.

Comparison of the theoretical infinite-back-shielded slab doses with the spherical doses of Fig. 12 and Table 2 shows that the slab approximation overestimates the doses at thin shields, but there is sufficient agreement at the thicker shields for spacecraft design purposes. This effect of the slab approximation is to be expected since shielding provided to a specific location by adjacent devices, experiments, spacecraft instruments, etc. will have the greatest impact on thinly shielded devices.

In the case of the n-channel biased devices, the theoretical spherical and the space flight experimental results have good agreement for the thin shields but are poorer for the thick shields (Fig. 20). However, the maximum difference is not greater than a factor of two. Clearly, the uncertainty in the environment models of a factor of two for protons and three for electrons can easily account for the disagreement. The experimental results of the shift in the threshold potentials of RCA biased n-channel devices for the 139 day environment suggest that the electron and proton environments are underestimated by the average environment model (the laboratory results of the shift in the threshold potentials are not produced by the space environment) or that the computational techniques are inaccurate. The shift of the threshold potentials under the thick shields are due only to the high energy protons, as shown in Fig. 11, and the techniques are more accurate for these particles than the electrons. However, this experiment cannot eliminate either explanation.

Modifications of the average environment models would provide a better fit to the data. Either the higher energy proton fluences must be increased and/or higher energy electrons must be included in the distribution to match the data. A change in the electron distribution to allow for the existence of more high energy electrons in the range of 2 to 8 MeV was tried in order to make the calculated and experimental results agree. However, it was found that an unreasonable increase in fluences by about two orders of magnitude was necessary together with the change in energy distribution. Consequently, it appears that an adjustment in the proton fluences by about a factor of 2 in the thick shield region, and by smaller factors in the thin shield region will make the results agree. The results for the 40 mil (1 mm) case are in good agreement, and therefore no change in the low energy proton fluences or the electron distribution is required.

10. Conclusions

The flight of the CREM experiment on board the Atmosphere Explorer-55 has been highly successful. All systems of the CREM instrument have been working well. From the preliminary results obtained so far the following may be concluded:

1. The CREM experiment has clearly demonstrated that C-MOS damage measurements made with simple radioactive sources in the laboratory, such as Co-60, may validly be used to predict changes in device properties affected by space environments consisting of charged particle fluxes (electrons and protons) distributed over wide energy ranges.
2. It has been verified, that spacecraft system survivability predictions using standard NASA models of the space radiation environment and conventional methods for dosage and shielding computation, are correct within a factor of two.
3. It has been shown, that the spherical dose calculation method will sufficiently well approximate, on the conservative side, the real exposure for nominal shield thicknesses from 50 mils (1.3 mm) to 100 mils (2.5 mm) of equivalent aluminum. For thicker shields this computational method yields results which are below those measured by a factor of two.
4. The experiment indicates, as a consequence of conclusion (3) for the thicker shields, that a more severe proton environment may exist during the AE-55 mission than predicted by the standard environment models, since above thicknesses of 100 mils (2.5 mm) only these particles contribute to the total dose. Considering that the proton models describe a mean solar maximum environment and that the AE-55 mission is flying during solar minimum, it is suggested that the proton environment during the inactive phase of the solar cycle is on the average higher by a factor of two than during solar max.

Acknowledgments

The CREM electronics box was designed and built by the Space Physics Research Laboratory of the University of Michigan. Dennis L. Haseltine was project engineer and Walter H. Pincus designed the analog circuitry. The CREM sensor assembly was designed and built at the Goddard Space Flight Center. David K. Studnick did the mechanical design and Dennis R. Hewitt did the thermal design.

Data acquisition software for the CREM experiment was done at Goddard Space Flight Center by William L. Mocarsky and Norman R. Beard, Jr..

The authors wish to thank AE Project Manager, David W. Grimes, AE Experiment Manager James A. Findlay and AE Project Scientist Nelson W. Spencer for their interest in and support of the CREM experiment.

The assistance of Mr. Sidney S. Brashears and Mr. Dae Ho Chang in conducting the CREM on-the-ground simulation experiment and plotting the data, is also greatly acknowledged.

References

1. Danchenko, V. and U. D. Desai, "Effects of Electric Fields and Their Configurations on Thermal Annealing of MOSFETs and Radiation Hardening", Symp. on Rad. Effects in Semicond. Components, Toulouse, France, March 1967.
2. Hassit, A., and C. E. McIlwain, "Computer Programs for the Computation of B and L (May 1966)", Data User's Note NSSDC 67-27, National Space Science Data Center, Greenbelt, Maryland, March 1967.
3. Stassinopoulos, E. G., and G. D. Mead, "ALLMAG, GDALMG, LINTRA: Computer Programs for Geomagnetic Field and Field-line Calculations", NSSDC 72-12, National Space Science Data Center, Greenbelt, Maryland, February, 1972.
4. Cain, J. C., and S. J. Cain, "Derivation of the International Geomagnetic Reference Field (IGRF 10/68)", NASA Technical Note TN D-6237, August, 1971.
5. Stassinopoulos, E. G., and C. Z. Gregory, "UNIFLUX: A Unified Orbital Flux Integration and Analysis System", to be published in 1976.
6. Teague, M. J., and J. I. Vette, "A Model of the Trapped Electron Population for Solar Minimum", NSSDC 74-03, National Space Science Data Center, Greenbelt, Maryland, April, 1974.
7. Lavine, J. P., and J. I. Vette, Models of the Trapped Radiation Environment, Volume V: Inner Belt Protons, NASA SP-3024, 1969.
8. Lavine, J. P., and J. I. Vette, Models of the Trapped Radiation Environment, Volume VI: High Energy Protons, NASA SP-3024, 1970.
9. Teague, M. J., and E. G. Stassinopoulos, "A Model of the Starfish Flux in the Inner Radiation Zone", NASA-GSFC Report X-601-72-487, December, 1972.
10. Brucker, G. J., R. S. Ohanian, and E. G. Stassinopoulos, "Successful Large-Scale Use of CMOS Devices on Spacecraft Traveling Through Intense Radiation Belts", IEEE Trans. On Aerospace and Electronic System, Vol. AES-12, No. 1, January, 1976.
11. Liley, B., and S. C. Hamilton, Modified Volume Dose Program (MEVDP), North American Rockwell Eng. Technical Report AFWL-TR-69-68, March 1971.
12. Private Communication with Captain D. Hollars, Air Force Weapons Laboratory (AFWL), June 1976.

13. Private Communication with Lt. J. Morel, Air Force Weapons Laboratory (AFWL), June 1976.
14. Halbleib, Sr., J. A. and W. H. Vandevender, "TIGER: A One-Dimensional Multilayer, Electron/Photon Monte Carlo Transport Code", SLA-73-1026; Sandia Laboratories, March 1974.
15. Danchenko, V., U. D. Desai, and S. S. Brashears, "Characteristic of Thermal Annealing of Radiation Damage in MOSFETs", J. Appl. Phys., 39, 2416 (1968).
16. Brucker, G. J., "Transient and Steady-State Radiation Response of CMOS/SOS", IEEE Trans. Nucl. Science, NS-21, 6, December 1974.

Table 1

AE-55: Orbit Integrated, Omnidirectional, Integral,
Vehicle Encountered Energetic Trapped Particle Fluxes

Energy (>Mev)	Electrons/cm ²			Protons/cm ²		
	Total Cumulative Intensities on Day			Total Cumulative Intensities on Day		
	48	88	139	48	88	139
.100	7.828 13	1.295 14	1.700 14	3.930 11	6.038 11	7.376 11
.250	1.745 13	2.890 13	5.000 13	1.309 11	2.086 11	2.653 11
.500	3.642 12	5.981 12	7.793 12	6.748 10	1.100 11	1.437 11
.750	1.381 12	2.250 12	2.850 12	5.155 10	8.492 10	1.121 11
1.000	7.161 11	1.166 12	1.492 12	4.335 10	7.190 10	9.250 10
1.250	4.446 11	7.216 11	8.600 11	3.653 10	6.100 10	8.045 10
1.500	2.764 11	4.472 11	5.654 11	3.060 10	4.430 10	7.000 10
1.750	1.847 11	2.986 11	3.700 11	2.610 10	4.414 10	6.003 10
2.000	1.235 11	1.994 11	2.546 11	2.200 10	3.640 10	5.200 10
2.250	8.500 10	1.340 11	1.750 11	1.878 10	3.214 10	4.438 10
2.500	5.736 10	9.284 10	1.171 11	1.704 10	2.920 10	4.037 10
2.750	2.500 10	5.000 10	6.500 10	1.560 10	2.670 10	3.700 10
3.000	8.928 9	1.472 10	1.899 10	1.412 10	2.422 10	3.354 10
3.250	2.630 9	4.334 9	5.500 9	1.280 10	2.200 10	3.080 10
3.500	7.752 8	1.278 9	1.657 9	1.169 10	2.009 10	2.775 10
3.750	2.288 8	3.779 8	4.850 8			
4.000	6.748 7	1.114 8	1.466 8			
4.250	1.908 7	3.138 7	4.000 7			
4.500	5.049 6	8.176 6	1.029 7			
4.750	9.393 5	1.390 5	1.556 6			

Table 2

AE-55: THEORETICAL SPHERICAL DOSES FOR 139 DAYS

IN ORBIT

<u>Device Location</u>	<u>Group 1 40 Mils</u>	<u>Group 2 80 Mils</u>	<u>Group 3 150 Mils</u>	<u>Group 4 300 Mils</u>
F1	19.39	10.5	5.61	4.07
F2	18.45	10.49	5.35	4.16
F3	19.6	9.8	5.83	3.81
F4	20.36	9.15	6.62	3.81
F5	9.14	7.65	6.08	3.77

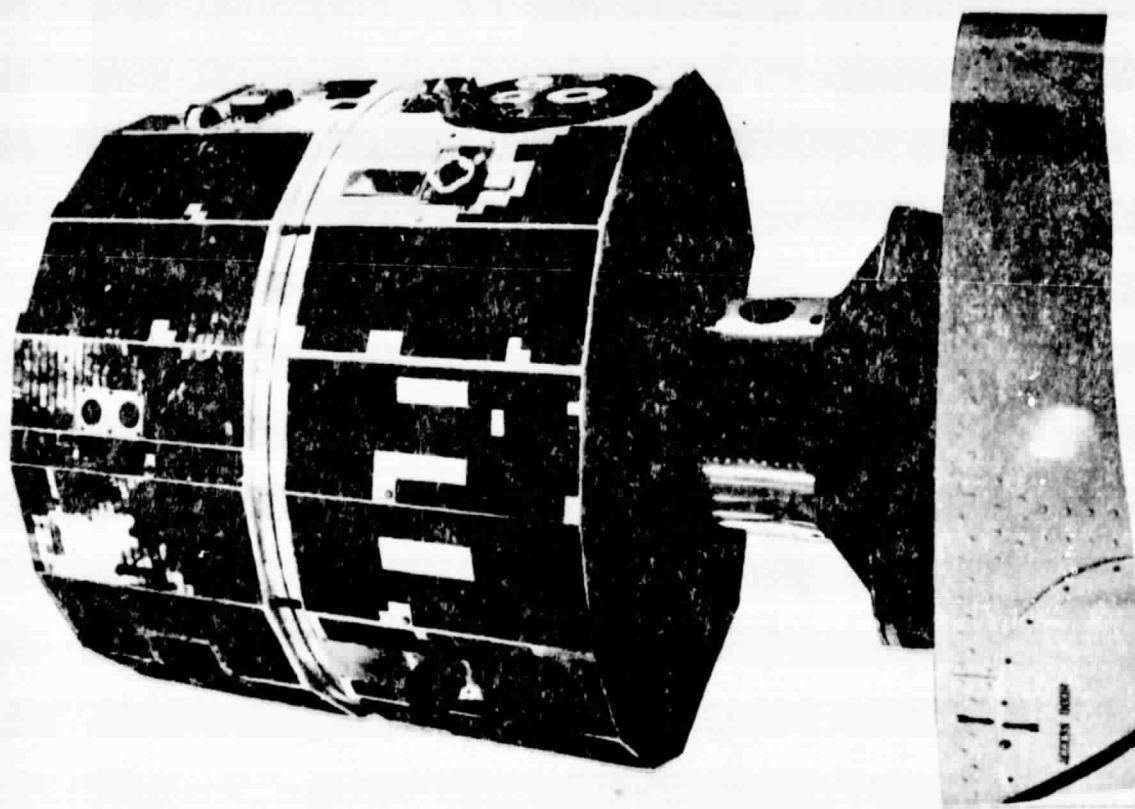


Fig. 1. Atmosphere Explorer-55 (AE-E)

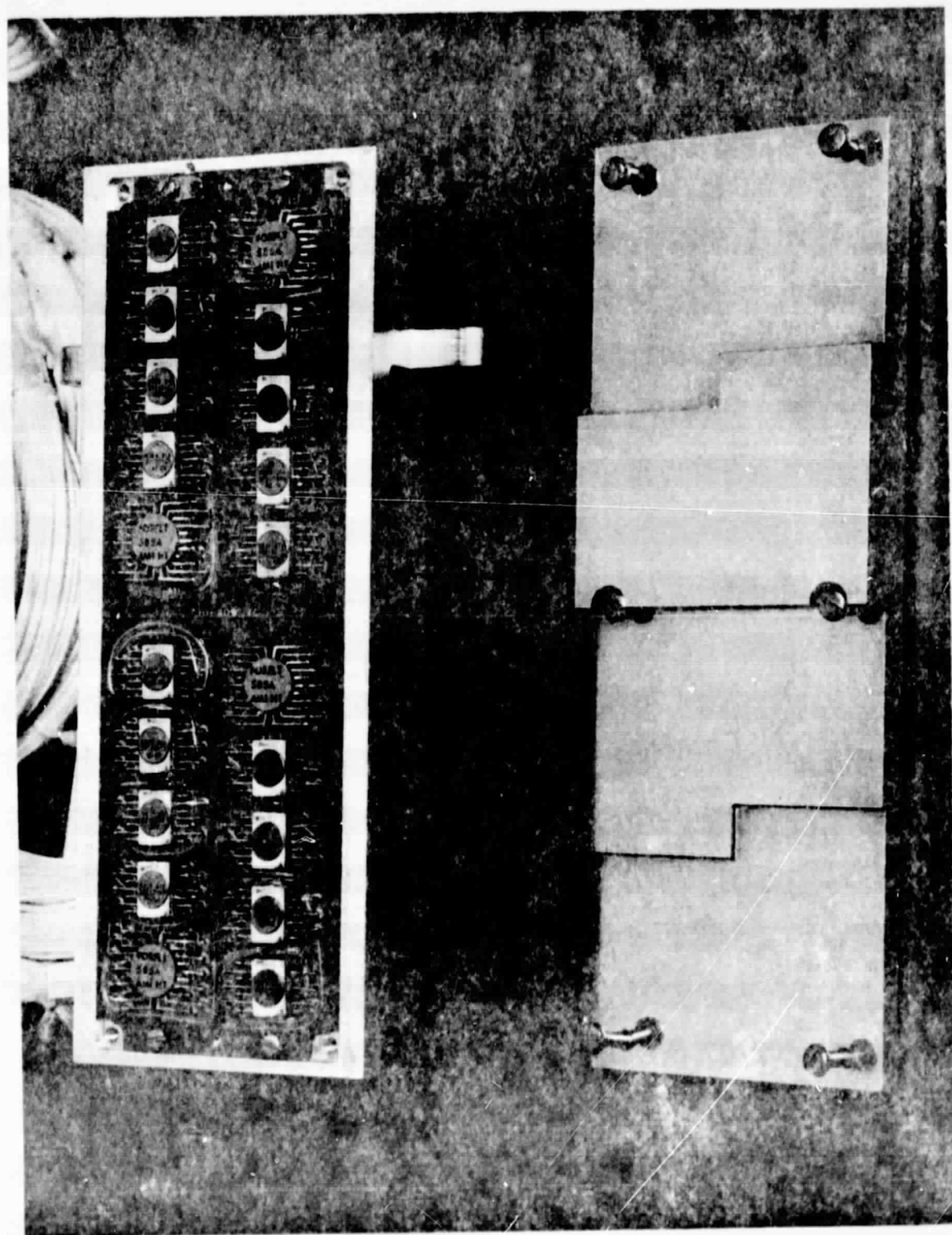


Fig. 2. CREM device box and its cover

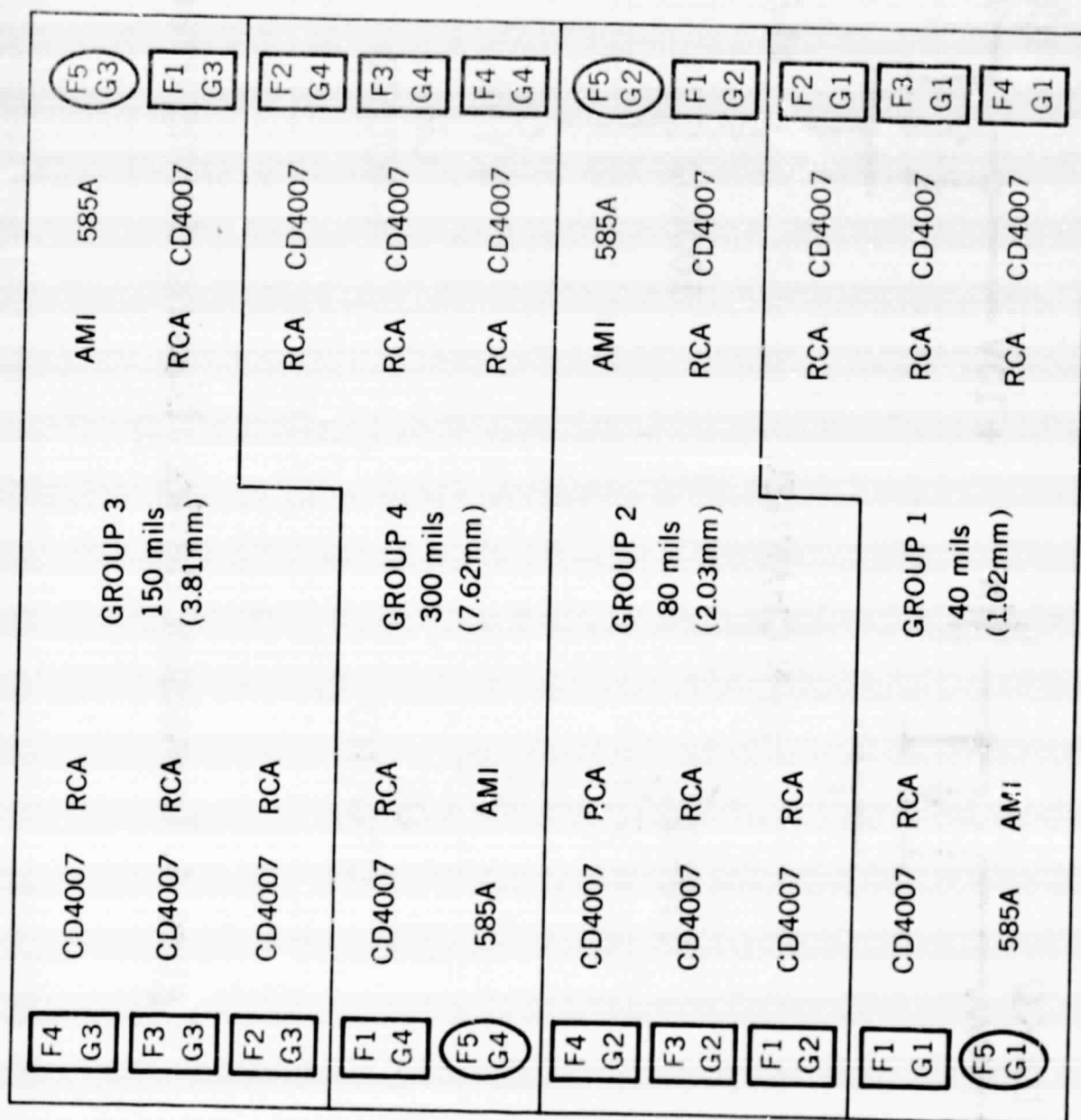


Figure 3. Device locations in CREM box.

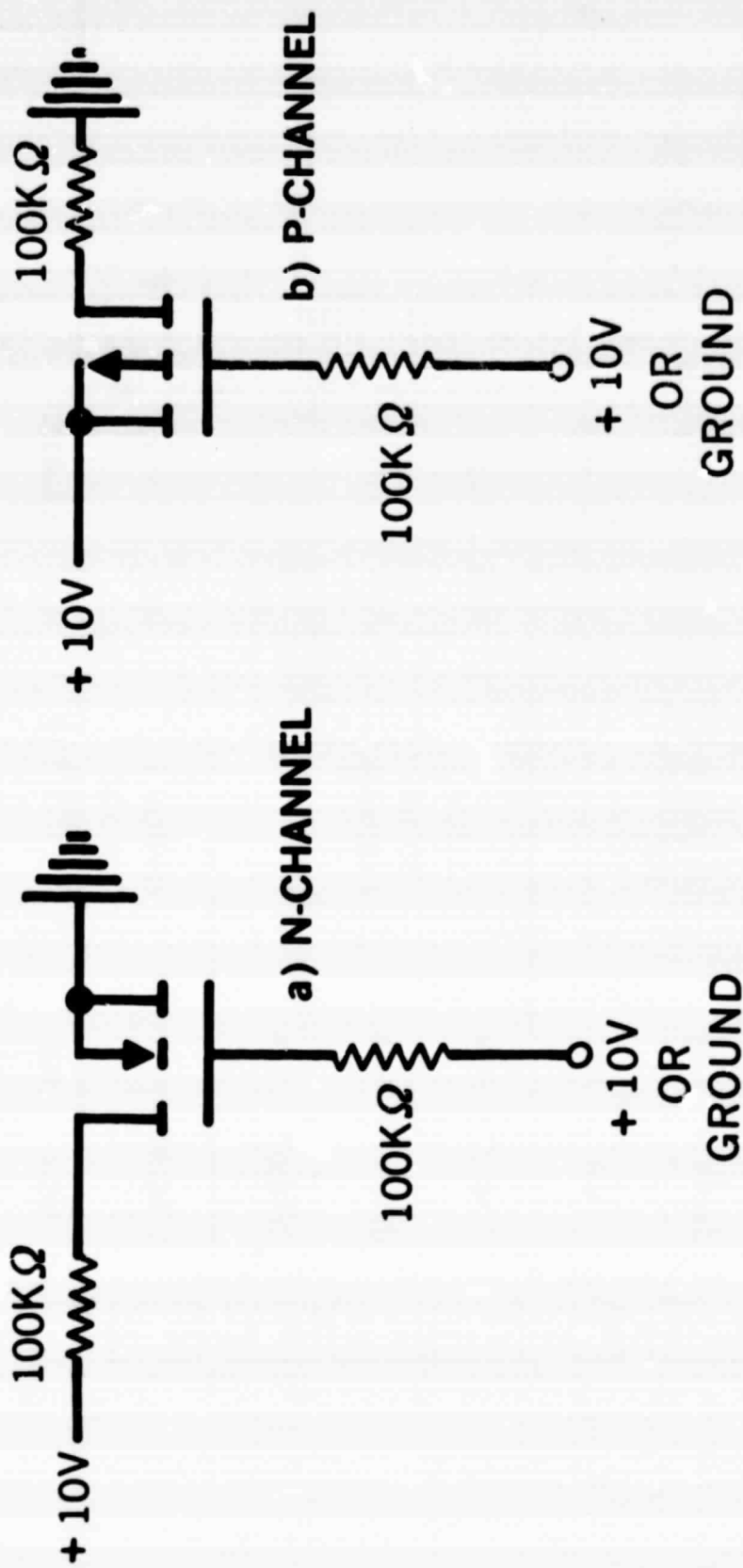


Figure 4. Transistor device biasing during irradiation.

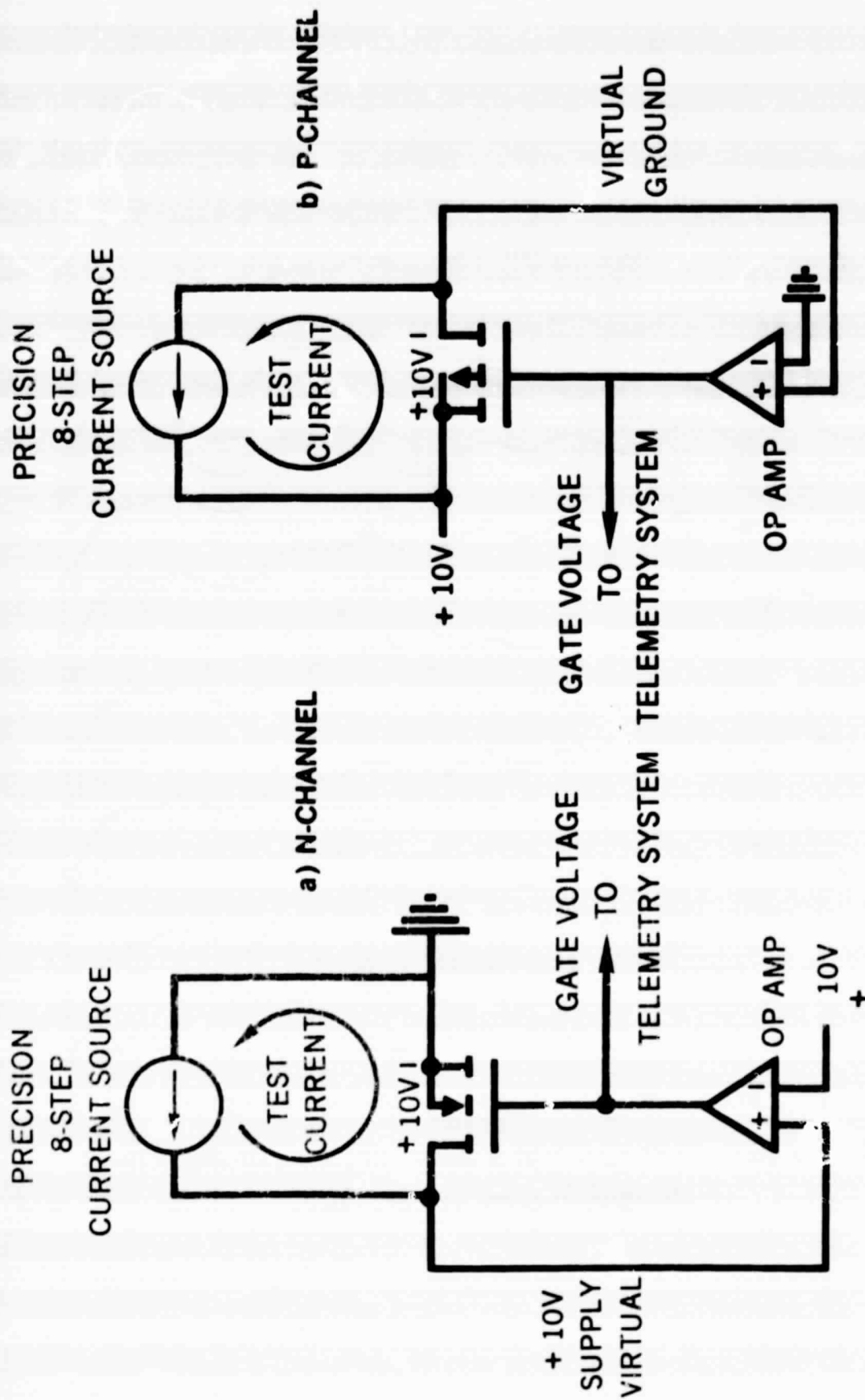


Figure 5. Transistor biasing during measurement.

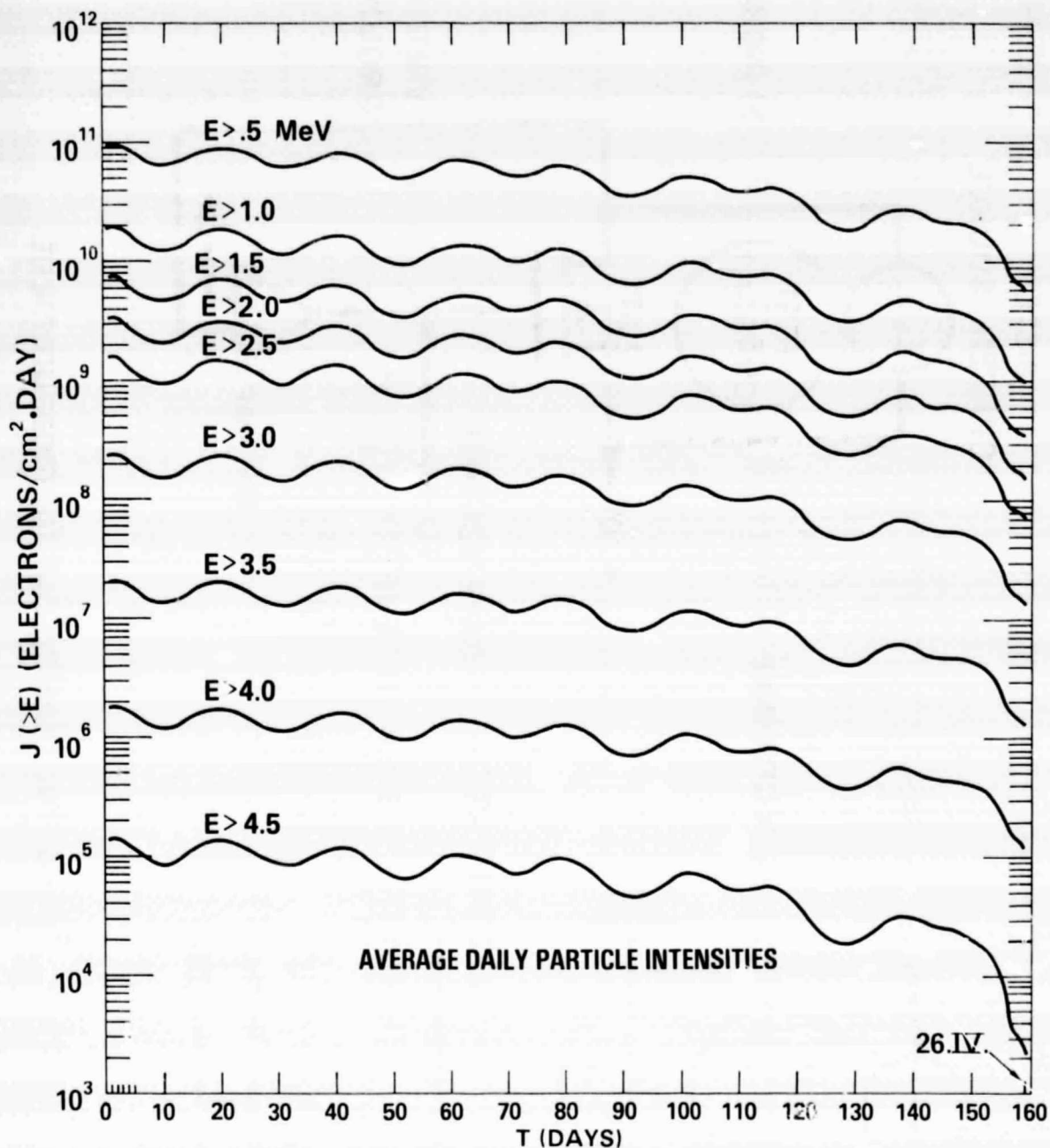


Figure 6. AE-E: Time History of Mission Integrated, Omnidirectional, Integral, Trapped Electron Fluxes

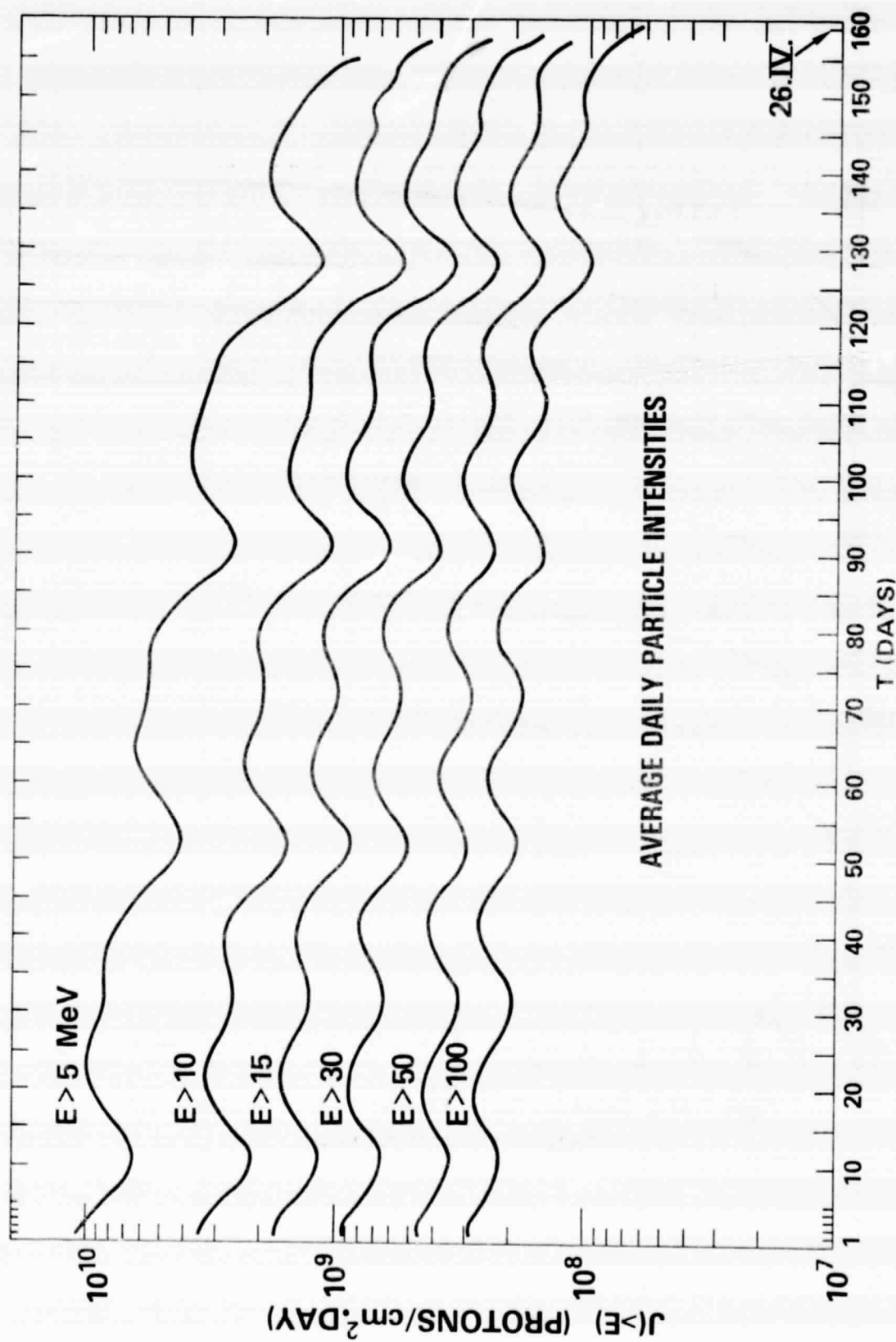


Figure 7. AE-E: Time History of Mission Integrated, Omnidirectional, Integral, Trapped Proton Fluxes

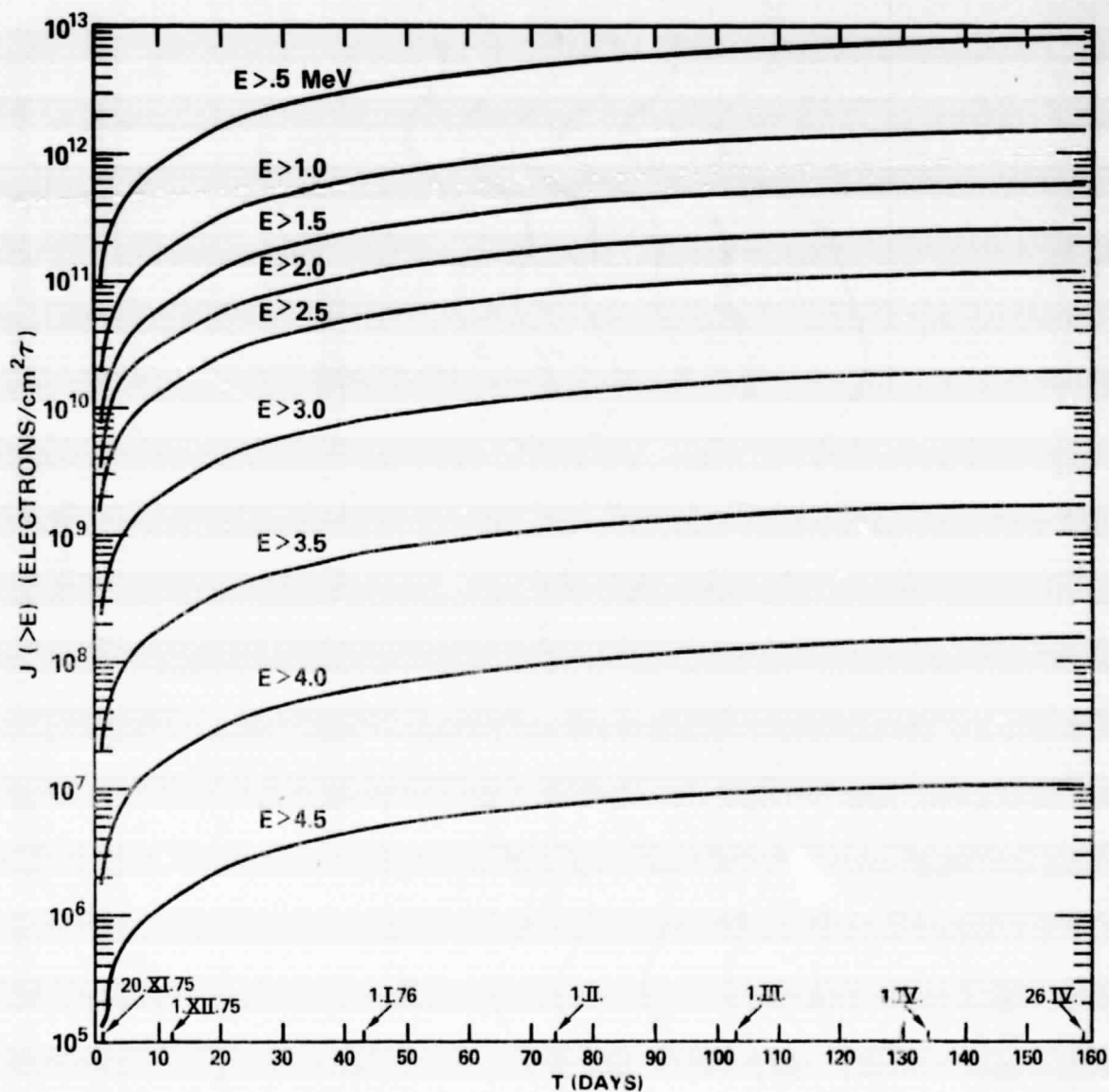


Figure 8. AE-E: Cumulative Sum of Mission Integrated, Omnidirectional, Integral Trapped Electron Fluxes

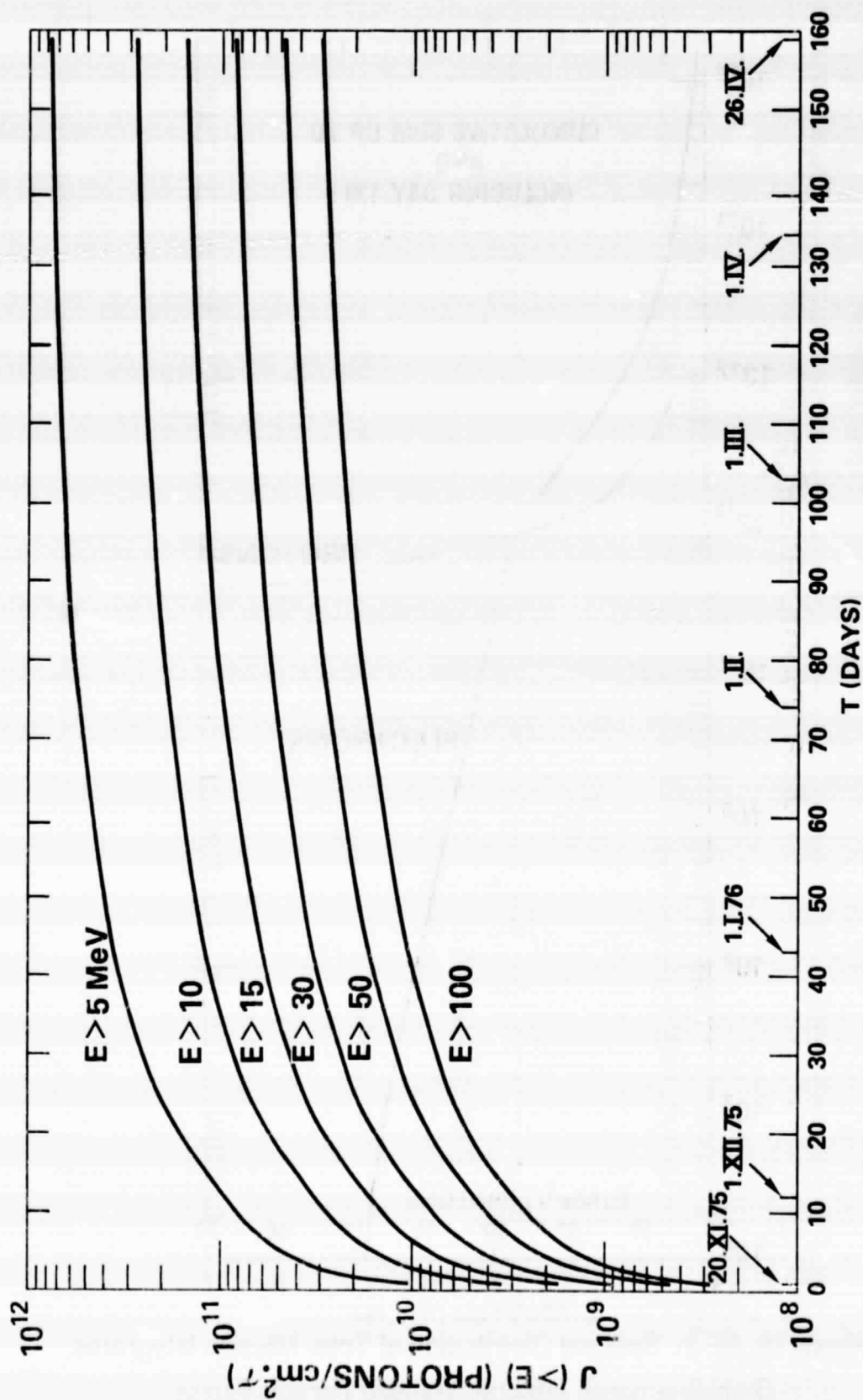


Figure 9. AE-E: Cumulative Sum of Mission Integrated, Omnidirectional, Integral, Trapped Proton Fluxes

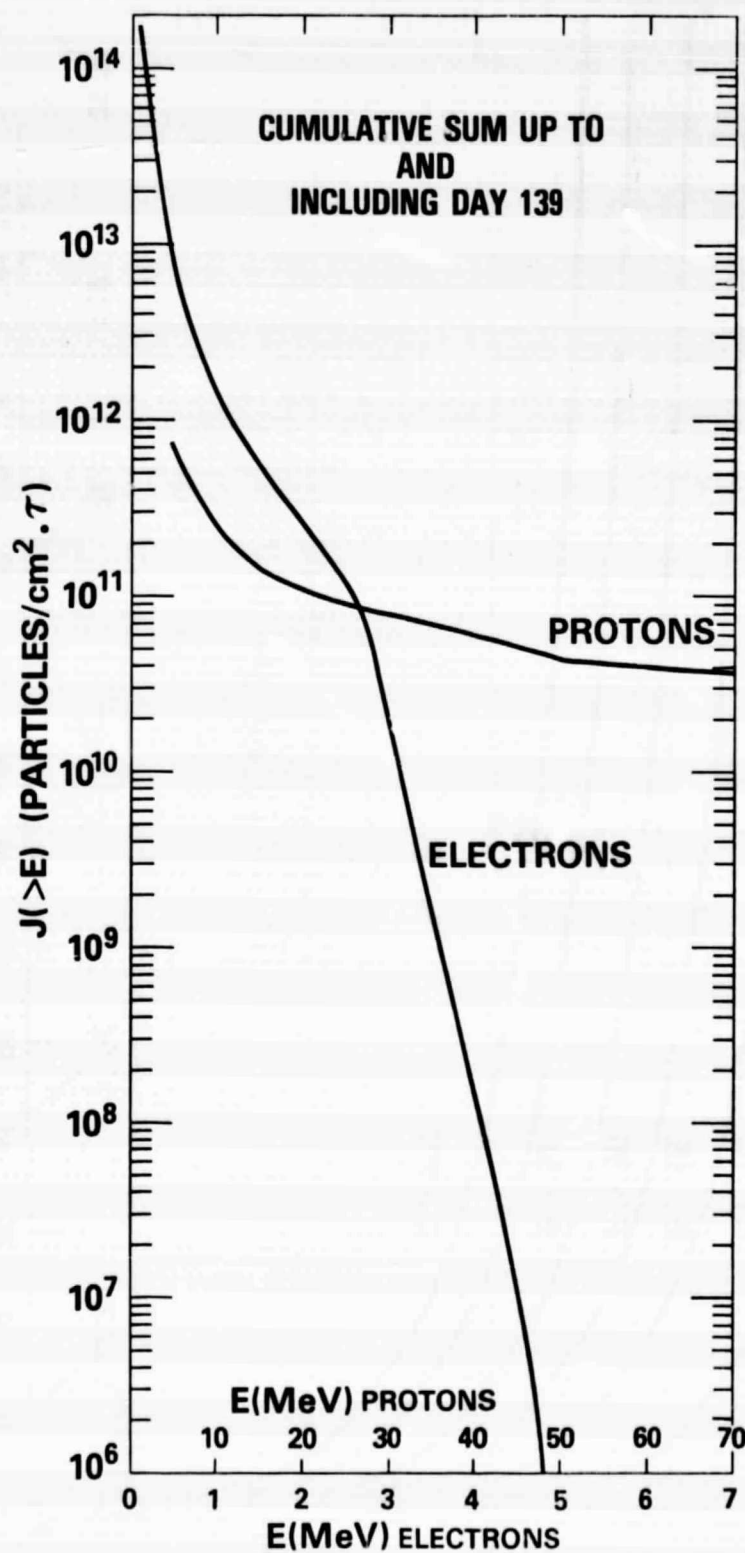


Figure 10. AE-E: Spectral Distribution of Total Mission Integrated, Omnidirectional, Integral, Trapped Particle Fluxes

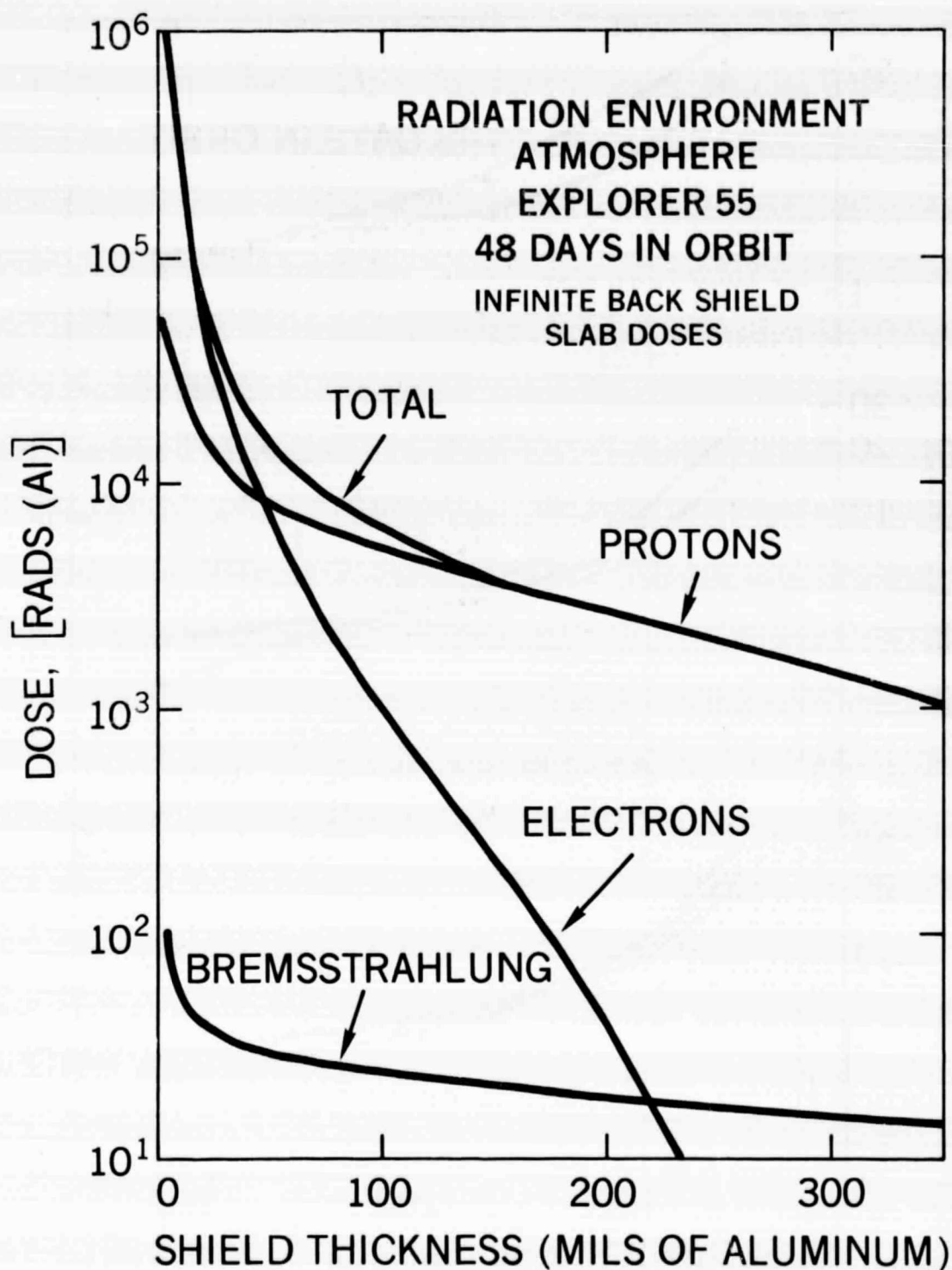


Figure 11. Contribution of electrons, protons, and Bremsstrahlung to the total dose-depth curve.

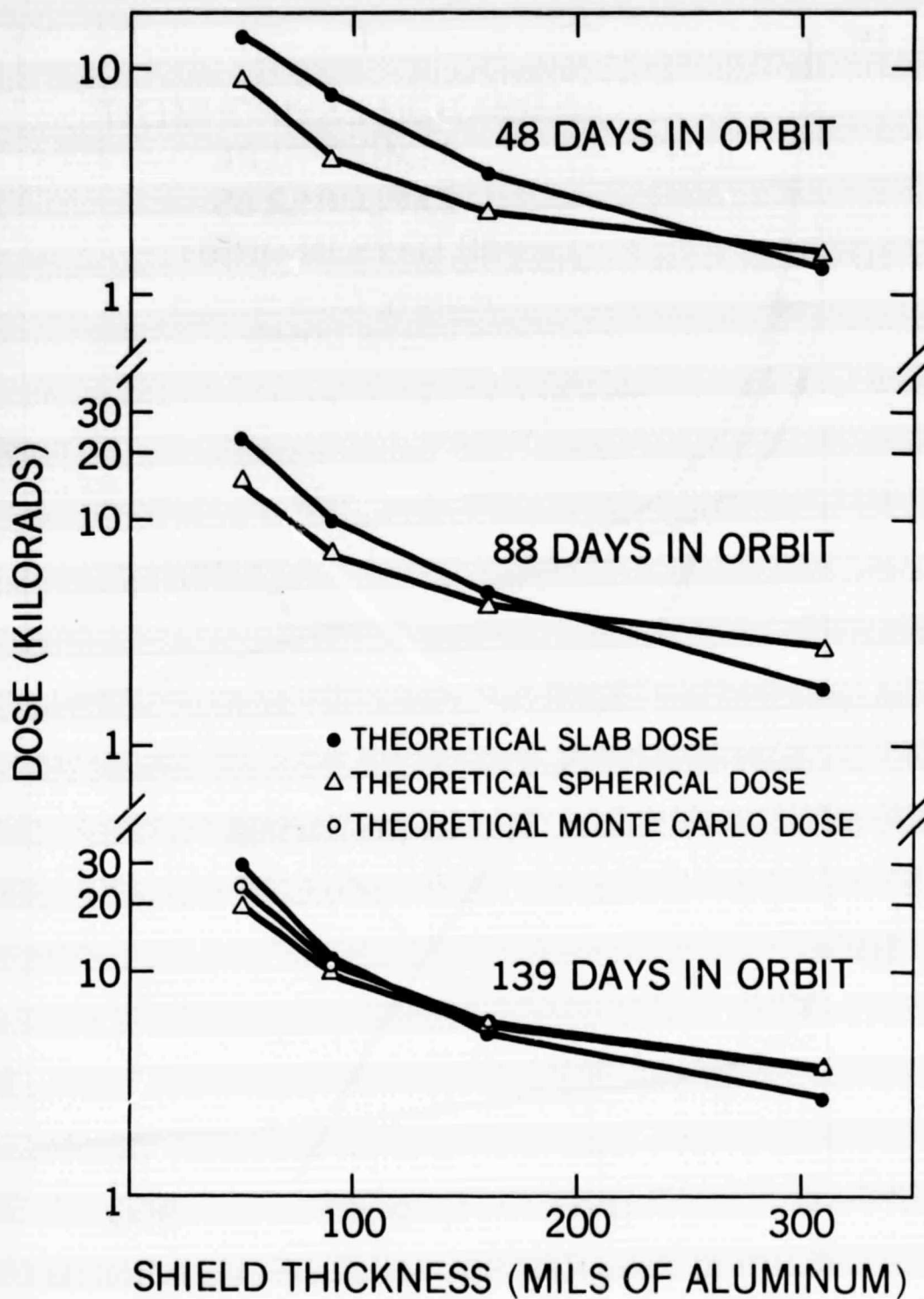


Figure 12. Dose-depth curves for slab and spherical geometries

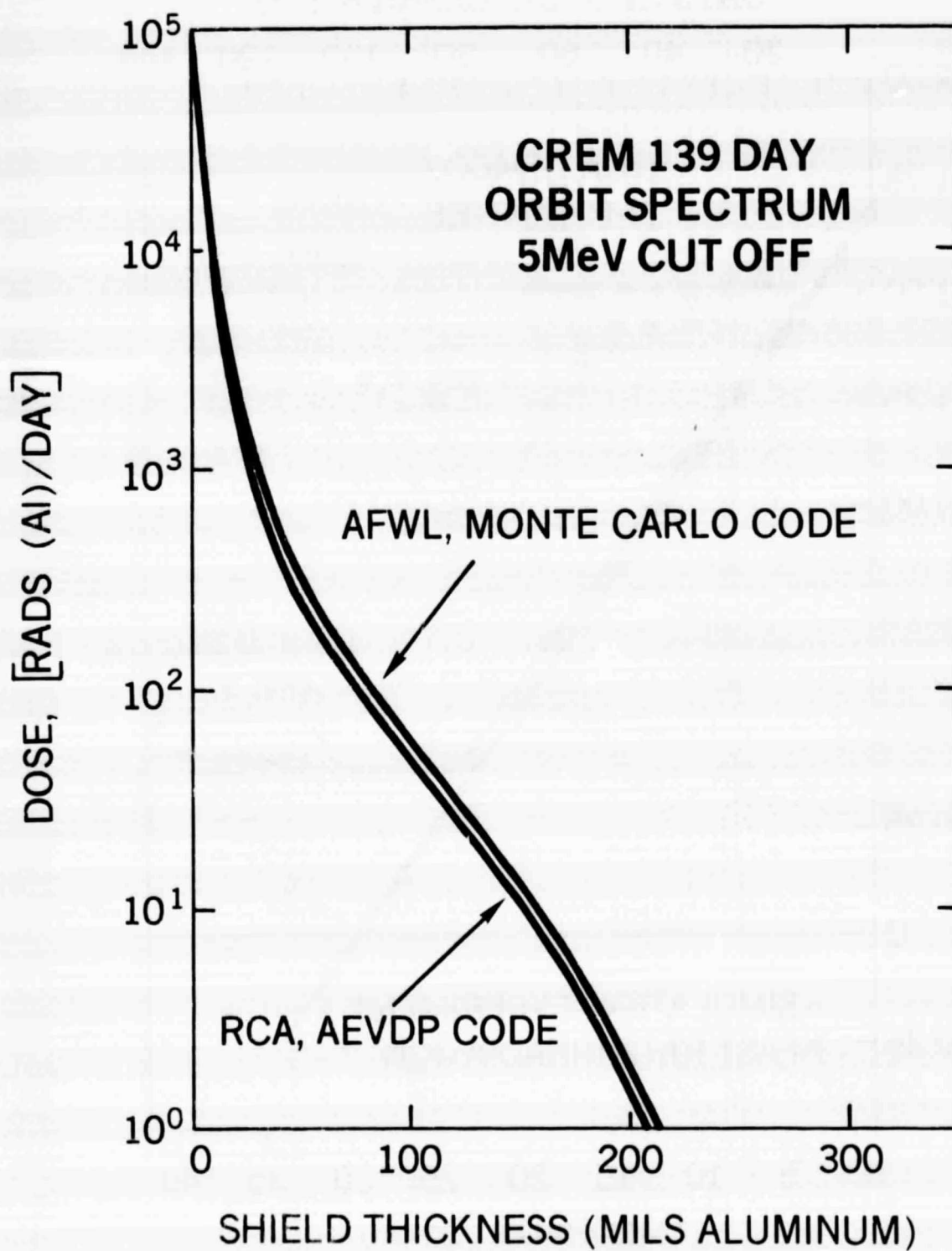


Figure 13. Monte Carlo and AEVDP dose-depth curves.

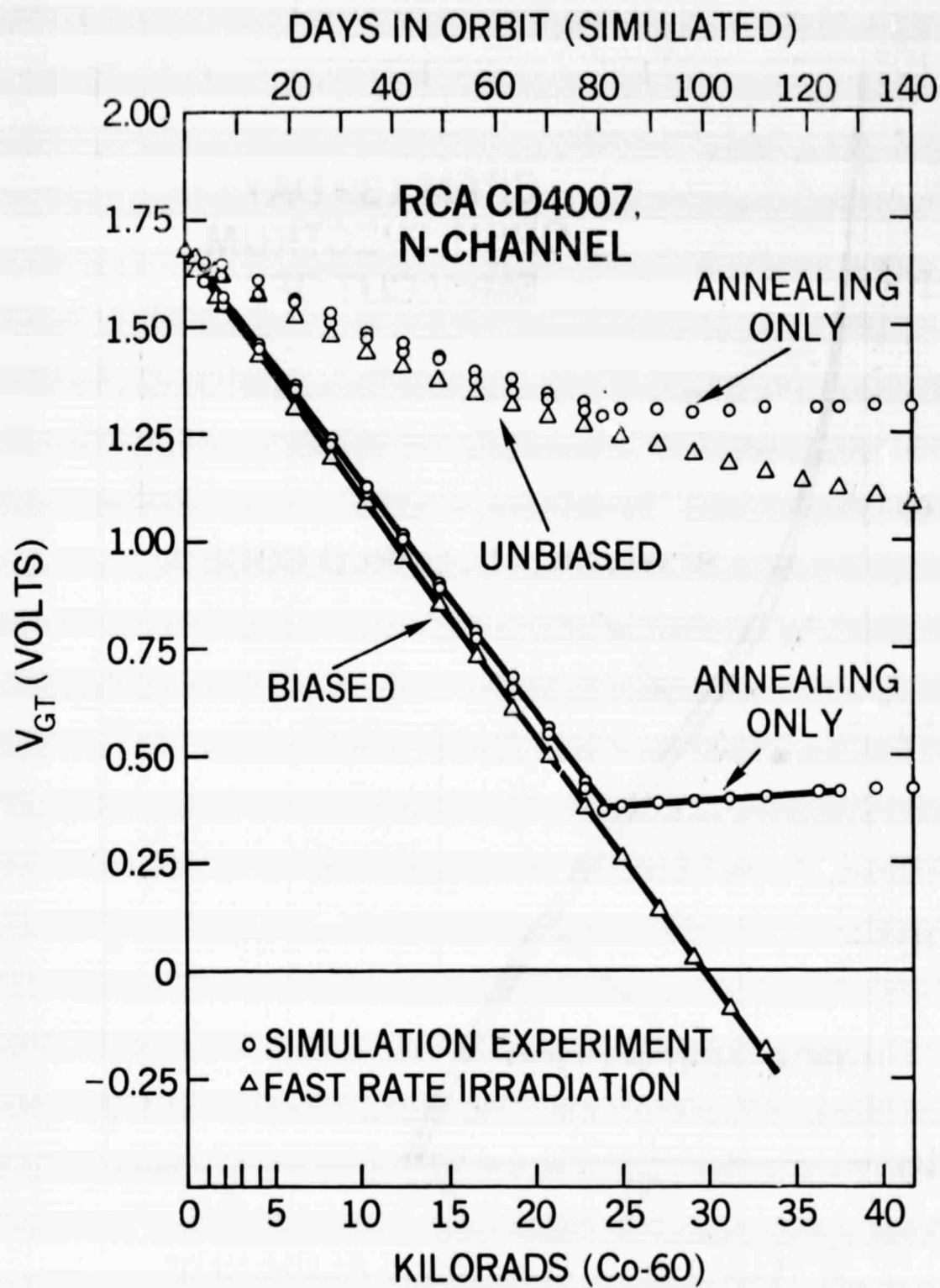


Figure 14. Radiation response of RCA n-channel transistor.

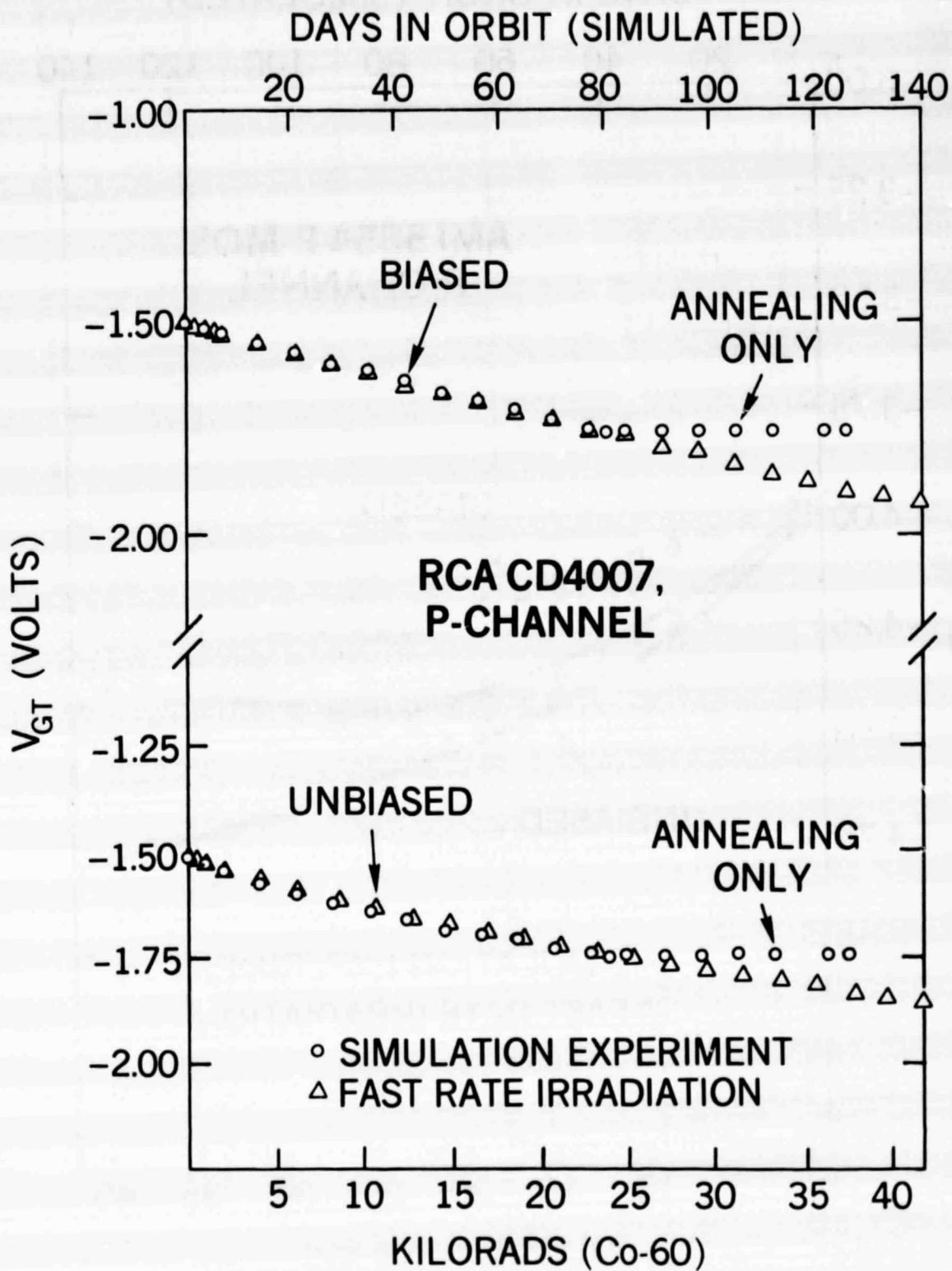


Figure 15. Radiation response of RCA p-channel

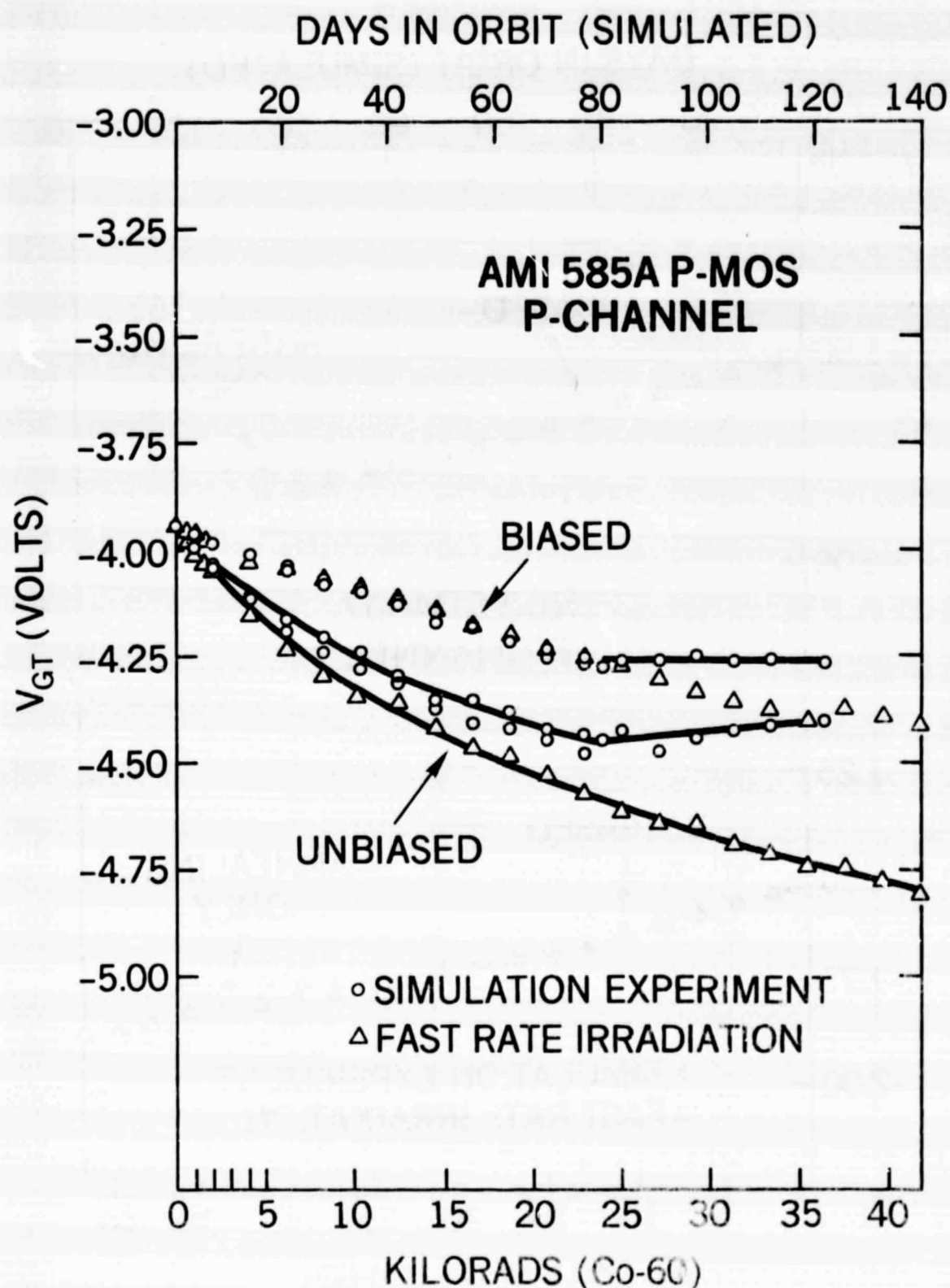


Figure 16. Radiation response of AMI p-channel transistor.

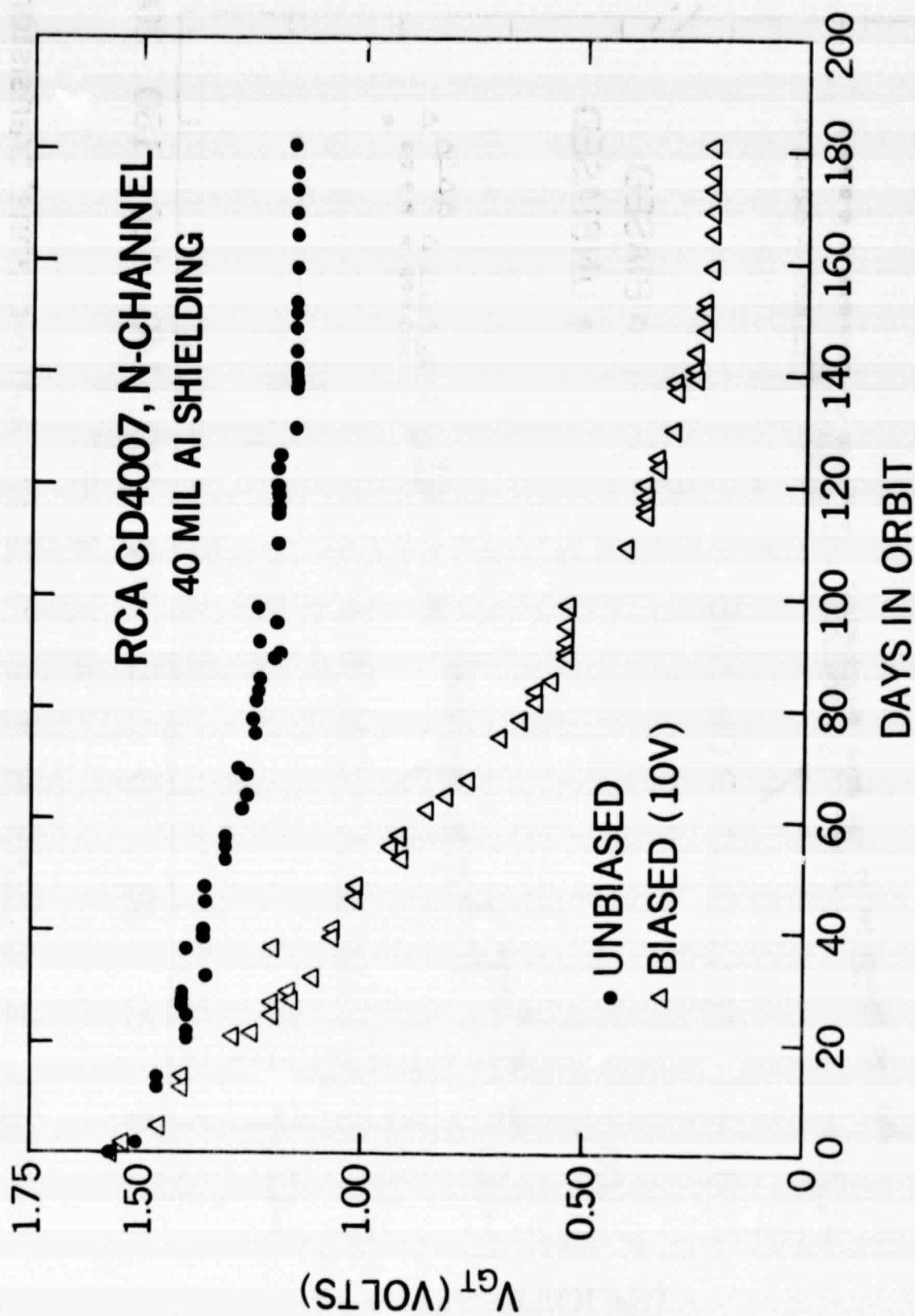


Figure 17. CREM flight data of RCA n-channel transistors.

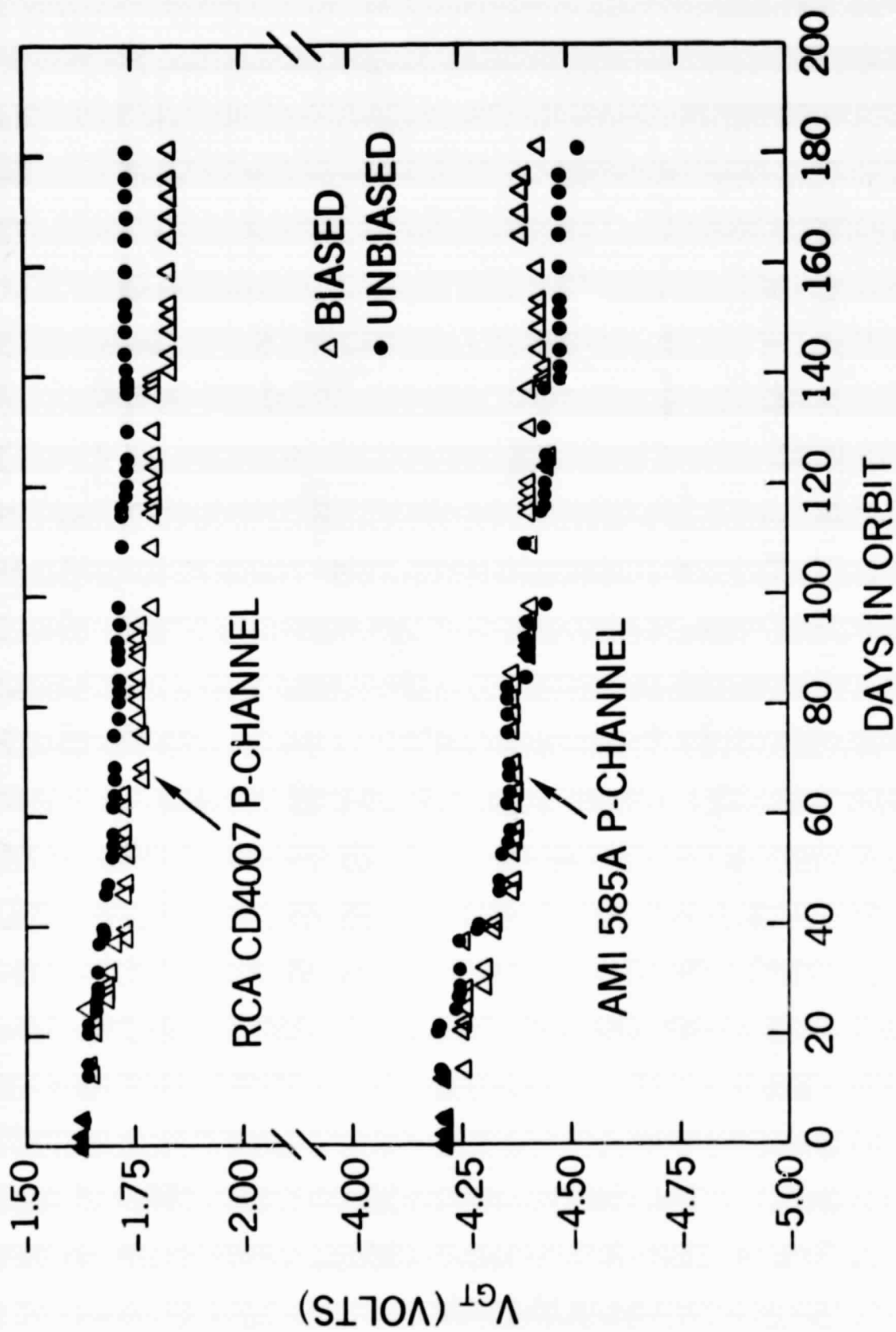


Figure 18. CREM flight data of RCA and AMI p-channel transistors.

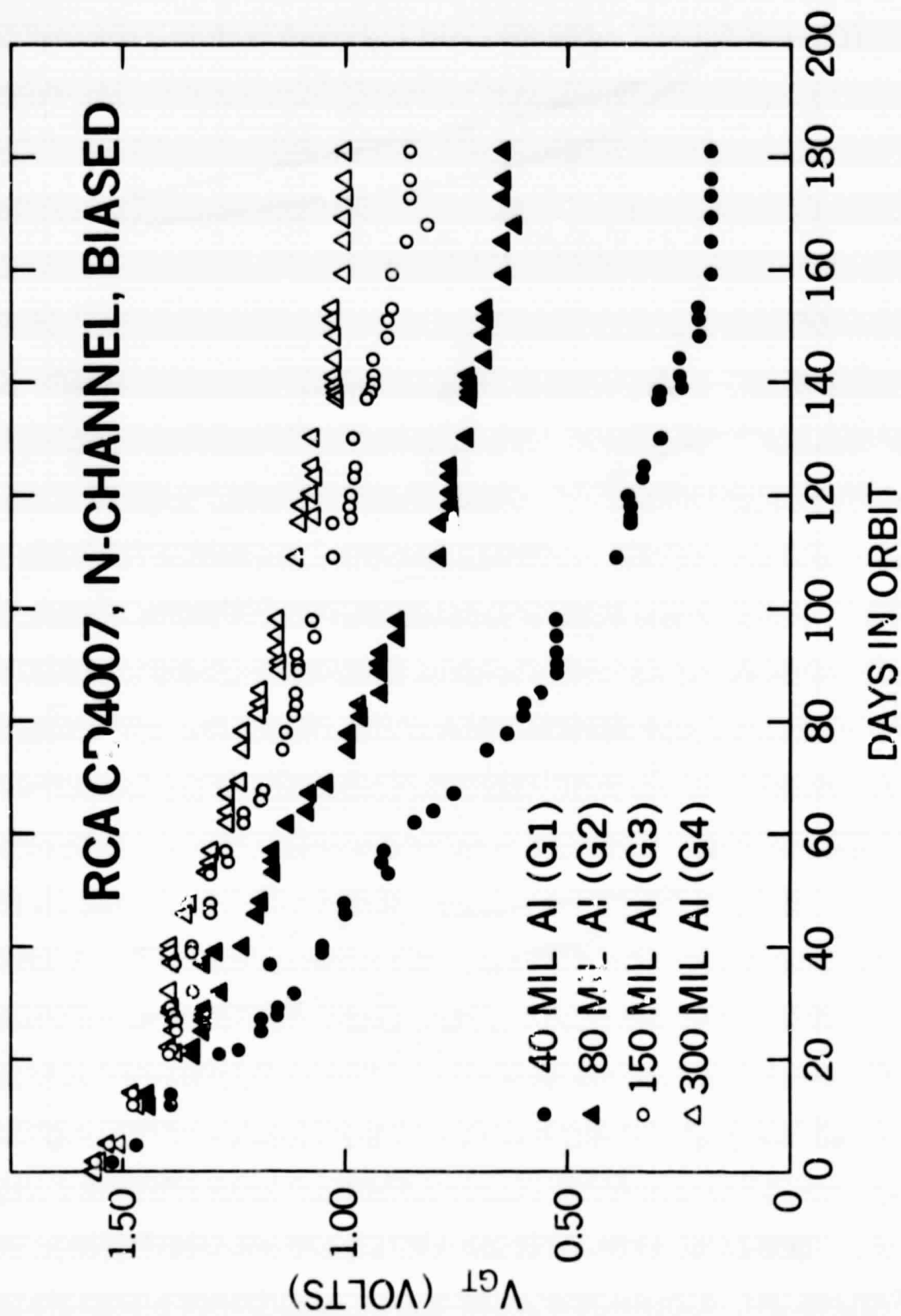


Figure 19. CREM flight data of RCA n-channel under various shields.

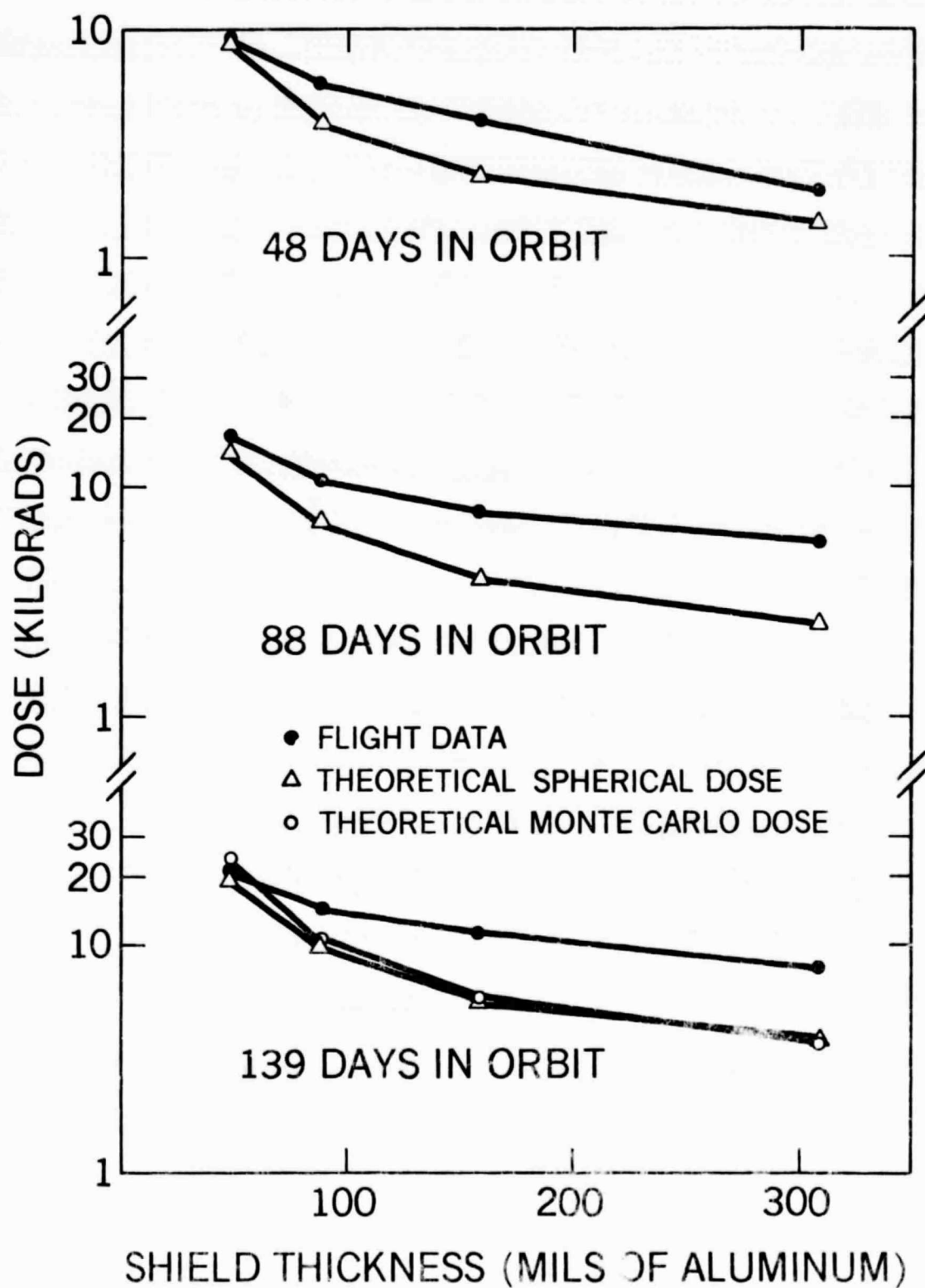


Figure 20. Comparison of flight and theoretical data.